University of Groningen

2D kinematics of simulated disc merger remnants

Jesseit, Roland; Naab, Thorsten; Peletier, Reynier F.; Burkert, Andreas

IMPORTANT NOTE: You are advised to consult the publisher's version (publisher's PDF) if you wish to cite from it. Please check the document version below.

Document Version
Publisher's PDF, also known as Version of record

Link to publication in University of Groningen/UMCG research database

2D kinematics of simulated disc merger remnants

Roland Jesseit,[1]★ Thorsten Naab,[1]★ Reynier F. Peletier[2]★ and Andreas Burkert[1]★

[1]*Universitäts Sternwarte München, Scheinerstr. 1, D-81679 München, Germany*
[2]*Kapteyn Astronomical Institute, University of Groningen, PO Box 800, 9700 AV Groningen, the Netherlands*

ABSTRACT

We present a 2D kinematic analysis for a sample of simulated binary disc merger remnants with mass ratios 1:1 and 3:1. For the progenitor discs we used pure stellar models as well as models with 10 per cent of their mass in gas. A multitude of phenomena also observed in real galaxies are found in the simulations. These include misaligned rotation, embedded discs, gas rings, counter-rotating cores (CRCs) and kinematic misaligned discs. Using the 2D maps we illustrate projection effects and the change in properties of a merger remnant when gas is included in the merger. We find that kinematic peculiar subsystems are preferably formed in equal-mass mergers. Equal-mass collisionless remnants can show almost no rotation, regular rotation or strong kinematic misalignment. The inclusion of gas makes the remnants appear more round (1:1) and axisymmetric (3:1). CRCs are almost exclusively formed in equal-mass mergers with a dissipational component. 3:1 remnants show a much more regular structure. We quantify these properties by applying the kinemetric methods recently developed by Krajnović et al. This work will help to understand observations of elliptical galaxies with integral field spectrographs, like SAURON.

Key words: methods: *N*-body simulations – galaxies: elliptical and lenticular, cD – galaxies: evolution – galaxies: formation – galaxies: fundamental parameters – galaxies: kinematics and dynamics.

1 INTRODUCTION

N-body simulations of mergers of disc galaxies have been very successful in reproducing many observational features of low and intermediate luminosity elliptical galaxies (Toomre & Toomre 1972; Barnes 1992; Hernquist 1992), while the most massive ellipticals are probably a result of collisionless early-type mergers or mixed mergers (Khochfar & Burkert 2003; Naab, Khochfar & Burkert 2006b). However, the observational information obtained from galaxies has been greatly enhanced with the advent of Integral Field Unit (IFU) instruments such as SAURON (Bacon et al. 2001), OASIS and GMOS. While mostly long-slit data were used to constrain the kinematic properties of early-type galaxies until recently, 2D data contain more information, and makes, for example, the detection of a second distinct kinematic component, which might be aligned with an angle not covered by a slit in a conventional observation, much easier or even possible at all.

The SAURON collaboration presented the first representative sample of 2D observations of elliptical and S0 galaxies (Emsellem et al. 2004, hereafter EM04). They presented 2D maps of line-of-sight velocities, dispersions and the third and fourth Gauss–

Hermite moments. These maps showed a multitude of features such as kinematically decoupled components (KDCs, see also Davies et al. 2001), central velocity dispersion dips, counter-rotating discs and many others. Dynamical modelling of the kinematic data revealed that galaxies with significant rotation are more anisotropic than slow-rotating ellipticals (Cappellari et al. 2005). An interesting new correlation was found that the slow-rotating ellipticals host large KDCs which have stellar populations of the same age as the main body, in contrast to fast-rotating ellipticals which have much smaller KDCs and are younger on average (McDermid et al. 2006). This correlation must contain some important information on the formation history of early-type galaxies.

Numerical studies of merging galaxies in the past showed that many peculiar kinematical features occur naturally in merger remnants, especially when a dissipational component was present in the progenitor galaxies. The dissipative component which can cool falls to the centre and changes the morphlogy of the remnant drastically by rearranging its orbital content (Barnes & Hernquist 1996). Disc like counter-rotating cores (CRCs) can also be formed from infalling gas, which has a spin vector with the opposite sign than the main rotating body (Hernquist & Barnes 1991), however also dissipationless scenarios have been proposed for counter-rotating stellar populations in early-type galaxies (Balcells & Quinn 1990; Balcells & González 1998; Bendo & Barnes 2000). Barnes (2002) showed that the gaseous material which does not fall into the centre

★E-mail: jesseit@usm.uni-muenchen.de (RJ); naab@usm.uni-muenchen.de (TN); peletier@astro.rug.nl (RP); andi@usm.uni-muenchen.de (AB)

can form large scale gas discs which can be warped or form bars. Polar-ring-like features have been successfully produced by several authors either in binary mergers (Bekki 1998), tidal accretion events (Bournaud & Combes 2003) or in a cosmological context (Macciò, Moore & Stadel 2006).

The aim of this work will be to compare 2D observations of a representative sample of 1:1 and 3:1 disc–disc merger remnants to the observations of the SAURON galaxy sample (EM04). The only similar study of this type was carried out by Bendo & Barnes (2000), who identified peculiar 2D kinematic features in collisionless merger models, such as an orthogonally decoupled core, counter-rotating populations and misaligned rotation. Their sample contained equal-mass mergers as well as mergers with mass ratios of 3:1 and they found that equal-mass mergers produce a larger variety of kinematical features. But as pointed out before, collisionless mergers are unlikely to be the only formation channel for early-type galaxies and it is unclear how the gas will influence 2D maps of such remnants. Gas infall also will vary from merging geometry to merging geometry as the gravitational torques on the gas will vary (Barnes 2002).

We will examine the merger sample of Naab, Jesseit & Burkert (2006a), hereafter NJB06, which includes for every merging geometry a collisionless merger and a merger where each progenitor galaxy had 10 per cent of its disc mass in gas. In total we study a sample of 96 mergers which should hopefully give us a similar variety of kinematic features than found in the SAURON sample. As we can compare the mock observations of each collisionless remnant with its gaseous counterpart, we can easily assess which kinematical feature was already present in the dissipationless remnant and which was caused by the influence of the gas.

Although 2D features can many times be intuitively grasped by visual inspection of the maps, this is hardly a quantifiable way to compare to simulations. Recently Krajnović et al. (2006), hereafter K06, developed a method to describe the properties of 2D maps of arbitrary moments of the line-of-sight velocity distribution (LOSVD). They termed this method *kinemetry* which works much in analogy to the common photometric fitting of isophotes. With this method one can determine, for example, in an easy way position angle, amplitude and shape of the rotation of a galaxy, or merger remnant, and identify kinematic subsystems more easily. The shape of the 2D maps are of course viewing angle dependant, and we try to take this into account by analysing the projections along the three principle axes. However, we are not carrying out a comprehensive statistical study in this work. We will use kinemetry throughout this work to quantify the kinematic features which arise through merging of disc galaxies.

In Section 2 we introduce the simulation sample. We explain the observational method to obtain 2D maps of various moments of the LOSVD in Section 3. The maps and their kinemetric analysis are presented in Section 4. We compare these results to 2D-kinematics of observed galaxies in Section 5 and summarize our findings in Section 6. Velocity maps and kinemetry of the whole sample are shown in Appendix A.

2 SIMULATIONS

The collisionless simulations are a subset of the simulations discussed in detail by Naab & Burkert (2003), hereafter NB03. The simulations with gas, which we use for our analysis are identical to the ones presented in NJB06. In the following we give only the most important simulation parameters.

Table 1. Properties of the modelled merger remnants. Special kinematical features observed and initial orientations of the progenitor discs are shown.

Model	Comment	i_1	i_2	ω_1	ω_2
11C1	High σ by counter-rotation	0	0	180	0
11C3	Regular rotation	0	0	71	−30
11C5	Low rotation	−109	−60	180	0
11C8	Surface-density change	−109	−60	71	90
11C12	Kinematic misalignment	−109	0	71	90
31C6	Regular rotation	−109	−60	71	30
11S2	Low σ ring	0	0	71	30
11S6	CRC in stars	−109	−60	71	30
11GS4	σ double peak	−109	−60	71	30
11GS9	Polar ring	−109	0	180	0
11GS16	CRC in gas	−109	60	71	90
31GS19	σ dumbbell	0	0	71	−30

The progenitor disc galaxies were constructed in dynamical equilibrium using the method described by Hernquist (1993). The system of units was: gravitational constant $G = 1$, exponential scalelength of the larger disc in the merger $h_d = 1$ (the scaleheight was $h_z = 0.2$) and mass of the larger disc $M_d = 1$. The discs were exponential with an additional spherical, non-rotating bulge with mass $M_b = 1/3$, a Hernquist density profile (Hernquist 1990) and a scalelength $r_b = 0.2h$, and a pseudo-isothermal halo with a mass $M_d = 5.8$, cut-off radius $r_c = 10h$ and collisionless core radius $\gamma = 1h$. The parameters for the individual components were the same as for the collisionless mergers presented in NB03. For this study we have resimulated the full set of 1:1 and 3:1 mergers with an additional gas component in the disc. We replaced 10 per cent of the stellar disc by gas with the same scalelength and an initial scaleheight of $h_{z,gas} = 0.1h_z$. This is in agreement with recent results from Khochfar & Silk (2006b) in which they show that merging progenitor galaxies at low redshifts contain on average 10 per cent gas for ellipticals more massive than 10^{10} solar masses. The gas was represented by smoothed particle hydrodynamics (SPH) particles assuming an isothermal equation of state, $P = c_s^2 \rho$, with a fixed sound speed of $c_s = 0.039$ in velocity units corresponding to $c_s \approx 10$ km s^{-1} if scaled to a Milky Way type galaxy. The N-body/SPH simulations were performed using the hybrid N-body/SPH tree code VINE (Wetzstein et al., in preparation) with individual time-steps.

The galaxies approached each other on nearly parabolic orbits, in agreement with predictions from cosmological simulations (Khochfar & Burkert 2006b), with an initial separation of 30 length units and a pericenter distance of 2 length units. The inclinations of the two discs relative to the orbit plane were i_1 and i_2 with arguments of pericenter ω_1 and ω_2. In selecting unbiased initial parameters for the disc inclinations we followed the procedure described by Barnes (1998). The initial orientations for the discs were the same as in NB03, Table 1. The merger remnants were allowed to settle into dynamical equilibrium for approximately 10 dynamical time-scales after the merger was complete. Then their equilibrium state was analysed.

The total sample comprises of 96 merger remnants of which half of them were run with a gaseous component. We adopt the following nomenclature for the mergers presented. The first two numbers give the mass ratio of the progenitor discs, that is, 11 or 31. The letter 'C' stands for analysing a collisionless merger (disc and bulge particles), 'S' stands for analysing only the stellar component of a gaseous merger (disc and bulge particles) and 'GS' analysing the total luminous part of a gaseous merger (disc, bulge and gas particles). The last number denotes the merging symmetry. For example, the

abbreviation 11C5 means: a collisionless equal-mass merger with merging symmetry 5. The mergers we have analysed in detail, a comment regarding their kinematic peculiarity and the detailed orbit parameters of the merger they resulted from, can be found in Table 1.

3 2D DATA ANALYSIS

3.1 LOSVDs

Every remnant was projected along the long axis (*X*-axis, *YZ* projection), the intermediate axis (*Y*-axis, *XZ* projection) and short axis (*Z*-axis, *XY* projection) of the moment of inertia tensor defined by the 40 per cent most tightly bound stellar particles. For the 2D analysis we binned particles within the central 3 length units on a grid of 48 × 48 cells. This corresponds typically to 2–3 effective radii depending on projection (see Naab & Trujillo 2006 for the exact determination of r_e). To include seeing effects we created for every luminous particle 10 × 10 pseudo-particles with identical velocities on a regular grid with a total size of 0.125 unit lengths centred on the original particle position. The mass of the original particle was then distributed to the pseudo-particles weighted by a Gaussian with a s.d. of 0.1625 unit lengths. Thereafter the pseudo-particles were binned on a 48 × 48 grid.

For the kinematic analysis we binned (mass weighted) all pseudo-particles falling within each grid cell in velocity along the line of sight. The width of the velocity bins was set to a value of 0.1 for line-of-sight velocities v_{los} in the range $-4 \leqslant v_{los} \leqslant 4$. This resulted in 80 velocity bins over the whole velocity interval. Using the binned velocity data we constructed line-of-sight velocity profiles (LOSVD) for each bin of the 2D grid. Subsequently, we parametrized deviations from the Gaussian shape of the velocity profile using Gauss–Hermite basis functions (Gerhard 1993; van der Marel & Franx 1993). The kinematic parameters of each profile (σ_{fit}, v_{fit}, H_3, H_4) were then determined simultaneously by least-squares fitting (Cretton et al. 2001; Naab & Burkert 2001b).

3.2 Kinemetry

Surface brightness and line-of-sight velocity are both moments of the stellar distribution function. The surface brightness is its zeroth-order and the line-of-sight velocity the first-order moment. However, there is a fundamental difference between the 2D fields of both moments: as the surface brightness is an even moment its iso-contours are point-symmetric (and therefore closed) and as the line-of-sight velocity is an odd moment its iso-contours are point-*anti*-symmetric and therefore open. While isophotal shapes were found to be very close to perfect ellipses, such a choice is not obvious for iso-velocity contours. K06 found empirically that the kinematics of early-type galaxies resemble very closely those of inclined discs, which in many cases can be well described by circular motion. If you would project a circular orbit which moves in the plane of the galaxy on the sky, then it would follow a simple cosine law:

$$V(R, \psi) = V_0 + V_C(R) \sin i \cos \psi, \qquad (1)$$

where *R* is the semimajor axis length of the projected circle on the sky, V_0 the systemic velocity, V_C is the ring circular velocity, *i* is the ring inclination and ψ is the azimuthal angle measured from the major axis of the ellipse (their equation 5).

However, as the authors state, elliptical galaxies are spheroids and not inclined discs and therefore their assumptions will be violated in nature. The next step is to see how far galaxies deviate from the simple cosine law. This can be achieved by the means of a Fourier series. A map of a moment of the LOSVD can be generalized to

$$K(a, \psi) = A_0(a) + \sum_{n=1}^{N} A_n(a) \sin(n\psi) + B_n(a) \cos(n\psi), \qquad (2)$$

where ψ is the eccentric anomaly and *a* the semimajor axis of the ellipse (their equation 6). K06 find that only few terms are needed (up to third order) to find a good description of the 2D data.

In the case of an even moment the fitting procedure is similar to what is done in conventional photometry, while in case of an odd moment their algorithm tries to minimize all terms of the harmonic expansion except $B_1(a) \cos(\psi)$, which according to their Ansatz carries the major contribution to the map of an odd moment of the LOSVD. In the first stage of the fit, these terms are minimized on a grid of position angles (Γ) and flattenings ($q = 1 - \epsilon$). After the ellipse, which describes the velocity profile best, has been found, the rotation curve is extracted again and Fourier-analysed to arbitrary order.

We follow the authors in using the following four parameters to quantitatively describe kinematic 2D maps: The already mentioned Γ, which measures the alignment of the rotation and *q* which can be interpreted as the opening angle of the iso-velocity contours. They argue that although the amplitudes of the separate cosine and sine terms in principle describe different properties of the maps, it is better for systems which are not axisymmetric to collect the amplitudes of sine and cosine terms of the same order (their equation 10):

$$k_n = \sqrt{A_n^2 + B_n^2}. \qquad (3)$$

For $n = 1$ we get the term k_1, which represents the amount of line-of-sight bulk rotation in case of a velocity map. The authors found that the ratio k_5/k_1, where k_5 is the first higher order term of the expansion which has not been fitted to the map and expresses the deviations from regular rotation, is sensitive to the presence of multiple kinematic components in a galaxy.

For a detailed description of their analysis method we refer the reader to the original paper (K06).

4 RESULTS

We show in this section the most important 2D maps of our sample in order to cover a broad range of differing kinematic features. The selection of these maps is again guided by, but not restricted to, the results of EM04. We will use the results of our previous study on the orbital structure of merger remnants (Jesseit, Naab & Burkert 2005, hereafter JNB05) and a kinemetric analysis for the interpretation of the maps. The apparent long axis of the remnants will be horizontally oriented for all the maps presented in this paper. In general we show maps for the collisionless stellar particles (C), the stars of the simulations with gas (S) and the stars in combination with gas (GS), as an indication of what the star would look like in the case of late star formation. The newly 'formed' stars would not have the same stellar mass-to-light ratio (M/L) than the 'old' stellar population. To account for this effect we adopt an ad hoc M/L following common stellar population models and modify the maps accordingly. During the merger a significant fraction of the gas falls to the centre (see NJB06) and overpowers the signal in the central bins and limits in some cases our interpretation of the results at very small radii. All the maps are shown in the original SAURON colour scheme, which was devised by M. Cappellari and E. Emsellem and is included in the KINEMETRY software distribution.
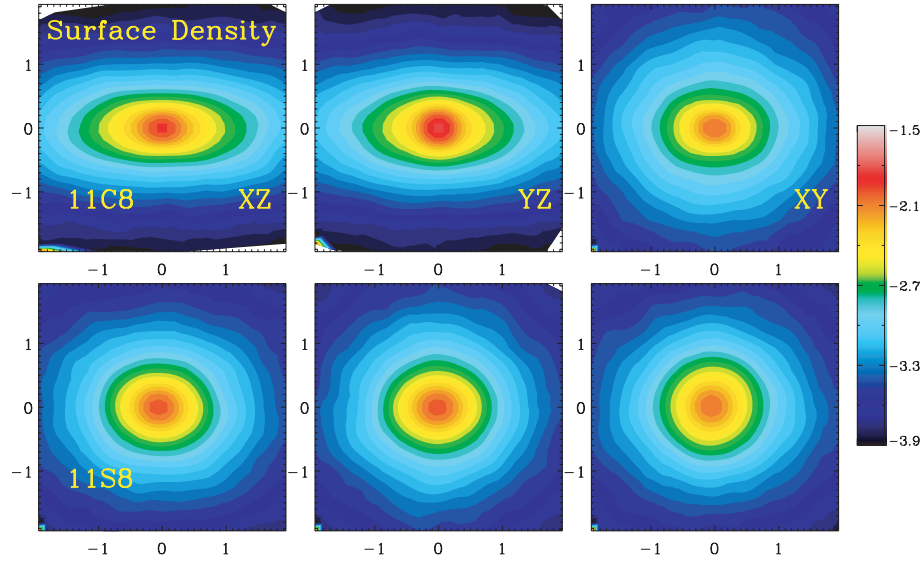
Figure 1. 2D surface-density maps for the equal-mass remnant with geometry 8. The projections along the three principal axes for the collisionless remnant (11C8, top row) are compared to the stellar component of the corresponding remnant with gas (11S8, bottom row). 11C8 is clearly triaxial whereas 11S8 is nearly round due to the influence of the additional gas component on the distribution of stars. One length unit corresponds to roughly one effective radius (Naab & Trujillo 2006). Colours indicate surface density in logarithmic scale.

4.1 Surface-density maps

It has been shown by a number of investigations that the presence of gas during a merger event makes the remnant more axisymmetric (Barnes & Hernquist 1996). NJB06 have shown that this effect is stronger for 1:1 remnants which are intrinsically more triaxial (or prolate) than 3:1 remnants. Fig. 1 shows this effect for the 2D stellar surface-density distribution of a collisionless 1:1 remnant and its counterpart, simulated with gas. Just by eye it is obvious that this particular remnant becomes much rounder if gas is included. Its intrinsic b/a changes from 0.83 to 0.95, while c/a increases even more significantly from 0.51 to 0.81. This is one of the few remnants in which the major axis tube fraction increases compared to the collisionless case from 5 to 11 per cent. Next to minor axis tubes, also outer major axis tubes support potentials of spherical shape.

So an increase of this fraction is to be expected (for a detailed description of orbit classification in merger remnants see JNB05). The effect of gas on the surface-density maps of 3:1 remnants is in general hardly detectable (see Fig. 2) as the collisionless remnant is already rather axisymmetric.

4.2 Rotation of collisionless remnants

In Fig. 3 we show the line-of-sight velocity field of two collisionless 1:1 remnants and one collisionless 3:1 remnant 31C6 with regular rotation. The properties of 3:1 remnants do not change significantly with the initial disc orientations of the progenitors. Therefore this example is typical for this mass ratio. The remnant 11C3 shows also regular rotation, despite of being an equal-mass merger, albeit with a lower amplitude than 31C6. 11C3 is the 1:1 remnant with
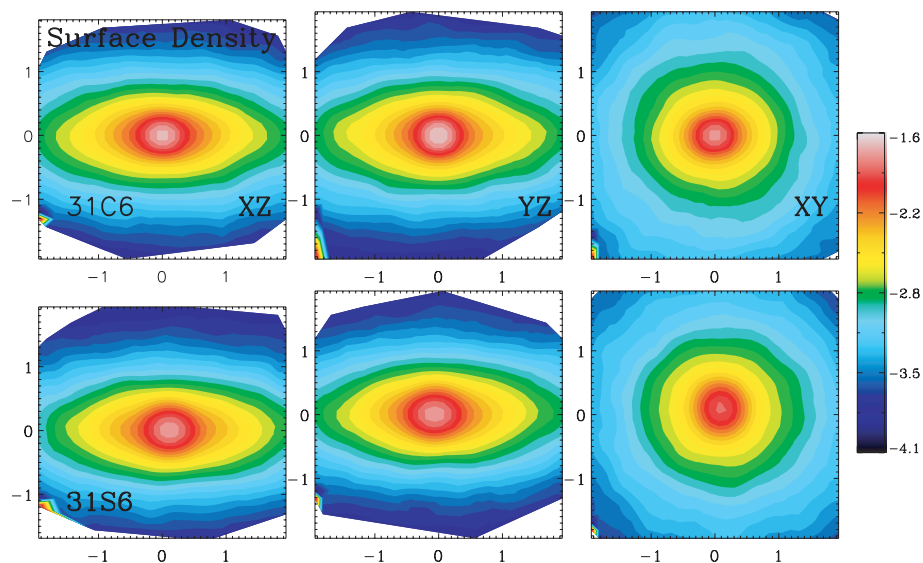
Figure 2. Same as Fig. 1 for the 3:1 merger with geometry 6. There is no obvious influence of gas on the stellar distribution.
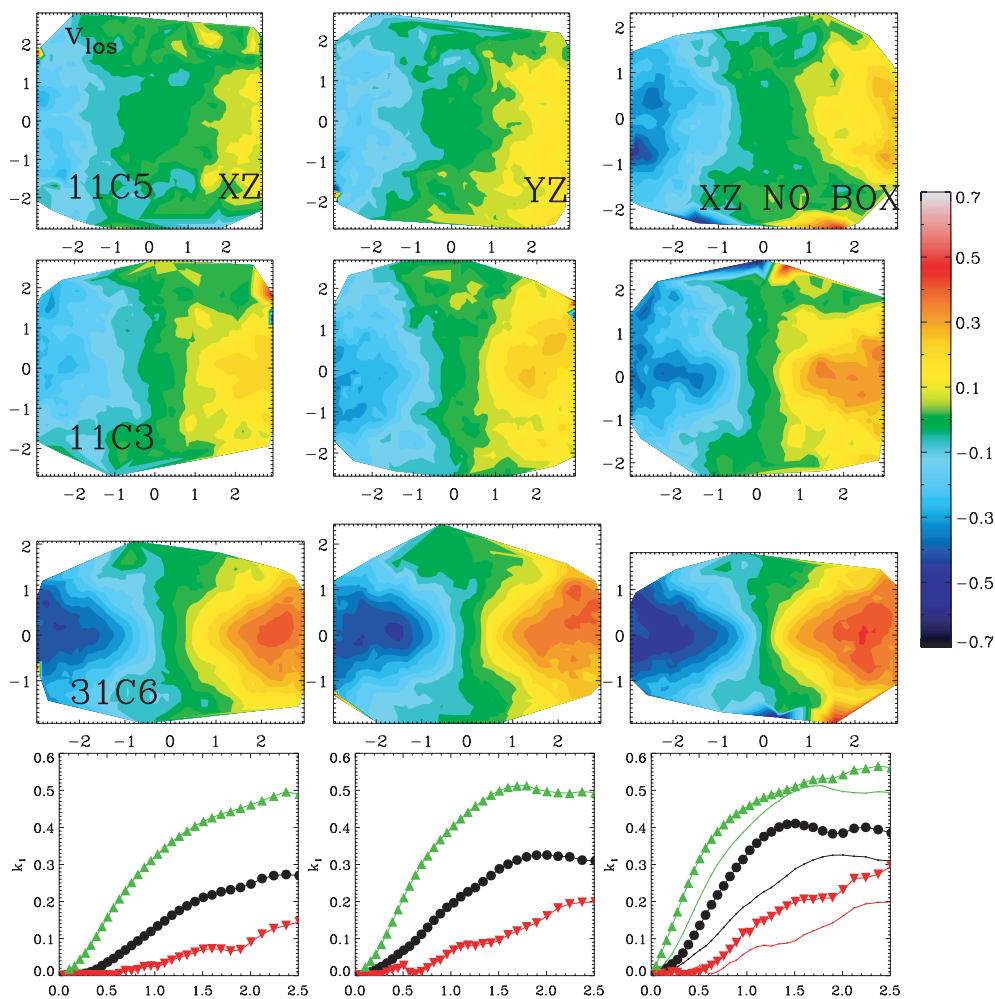
Figure 3. 2D line-of-sight velocity field for the collisionless 1:1 remnant 11C5 (top row), the 1:1 remnant 11C3 (second row) and the 3:1 remnant 31C6 (third row). The bulk rotation is indicated in the bottom row. 31C6 (green triangles) and 11C3 (black circles) show regular rotation, while 11C5 (red upside down triangles) has a large box orbit component and rotates very little. How the 2D maps of the remnants would look like with the box orbits removed is shown in the last column. The rotation curve without box orbits is plotted with thick symbols and for comparison the original rotation curve with thinner symbols (bottom right-hand panel). The net rotation increases significantly when the box orbits are removed.

the highest minor axis tube fraction, but it is rather an exception, as in general the rotational structure of equal-mass merger remnants is more complicated and depends on the initial disc geometry. In the most extreme case a 1:1 merger remnant can exhibit almost no rotation within in an effective radius, like 11C5, which has the highest box orbit fraction of all merger remnants.

The kinemetry shows (Fig. 3, bottom row), as indicated before, that 11C3 and 31C6 have a rising bulk rotation, that is, k_1 curve, while 11C5 has almost no amplitude in the centre. We extract the box orbit population in each remnant, to see how this changes the maps. Mainly we observe now particles which have been classified as minor axis tubes, which have a significant amount of L_z. In every case the amount of rotation increases (bottom row, right-hand panel) and also the iso-velocity contours appear to be more closed. Still, all three maps are quite different in appearance. That means that in the merging process also the shape of the z-tubes is rearranged. They are considerably more 'puffed up' in equal-mass mergers than in unequal-mass mergers.

We want to note that the 2D velocity maps of 1:1 mergers are sometimes too complex to be fitted adequately with ellipses. Very low rotation causes the ellipse fitting algorithm to extract erratic

position angles. We therefore restrict ourselves to constant position angle of 0° and constant ellipticity of $q = 0.5$. See also discussion in Section 4.4).

4.3 The influence of gas on v_{los} and h_3

In Fig. 4 we show the 2D line-of-sight velocity map of a 3:1 remnant and the corresponding distribution of h_3. For the collisionless remnant (left-hand panels) v_{los} and h_3 are correlated inside $0.5r_e$ and anticorrelated in the outer parts. This behaviour is typical for collisionless remnants (Bendo & Barnes 2000; Naab & Burkert 2001a; NJB06) and is not consistent with observations of elliptical galaxies (Bender, Saglia & Gerhard 1994). The correlation of v and h_3 at the centre is caused by the superposition of box orbits and minor axis tubes in collisionless merger remnants. This happens because the peak of the total velocity profile at a radius close to the centre is significantly moved to lower velocities, with respect to the short axis tube population, because box orbits, having zero mean angular momentum, peak normally at zero mean velocity. Therefore the normally steep leading wing becomes broader (see NJB06 for a more detailed discussion). When we remove the box orbit component
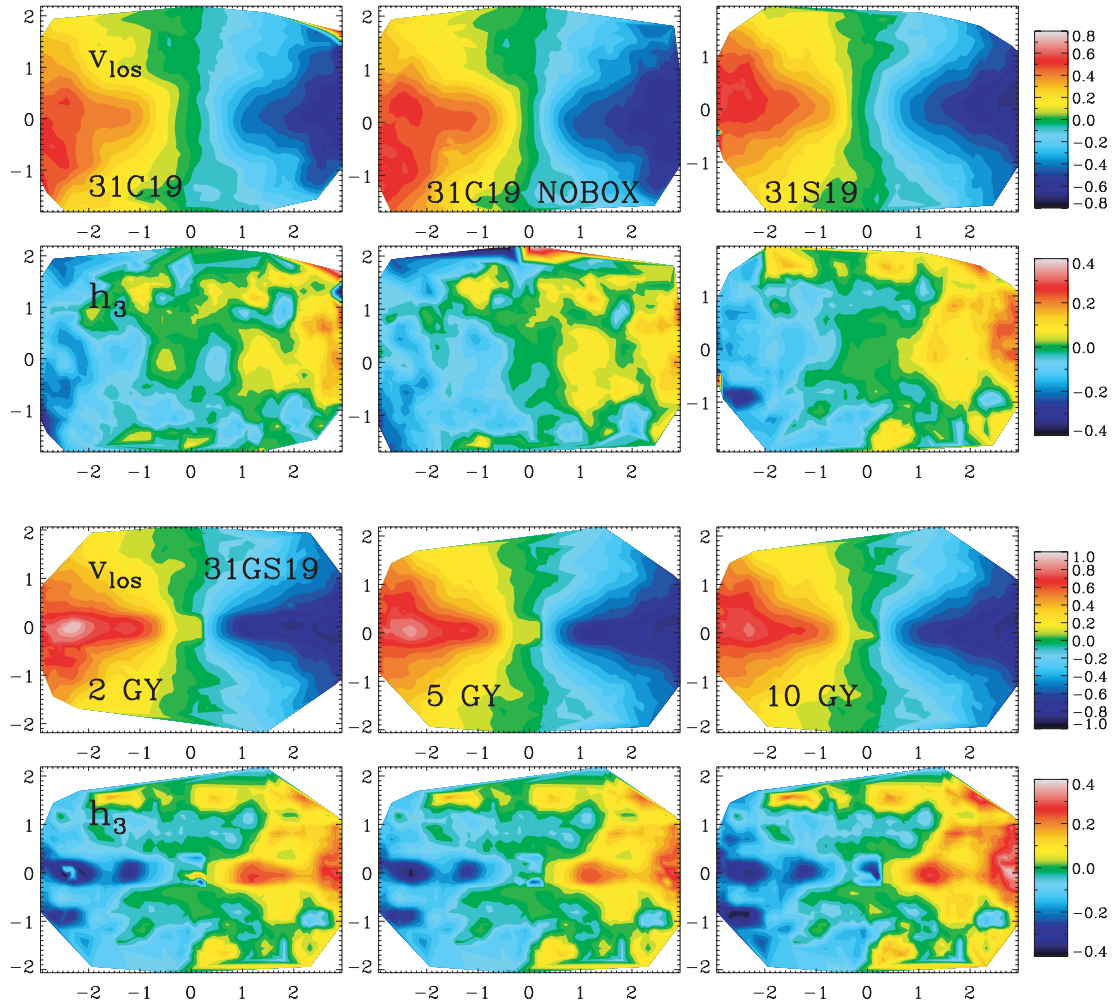
Figure 4. 2D maps of velocity and h_3 for the 3:1 remnant with geometry 19. For the collisionless remnant (31C19) v_{los} and h_3 is correlated in the inner parts and anticorrelated in the outer parts (top left-hand panel). This correlation vanishes, when the box orbits are removed (top middle). Gas similarly changes the orbital set-up and no correlation is visible in the stellar component of the gaseous remnant (top right-hand panel). If the gas is 'ad hoc' turned into stars the anticorrelation becomes even more visible (two bottom rows). Accounting for the lower M/L of the gas particles increases the peak velocity but changes hardly the structure of the h_3 maps.

and observe this modified remnant, the correlation at the centre has disappeared (Fig. 4, top middle panel).

If gas is present during the merger the correlation at the centre disappears even if only the stellar component is considered (4, top row, right-hand panel), leading to an overall anticorrelation which is even stronger if we include the gas component in the analysis (two bottom rows). The gas influences the kinematic structure of the remnant twofold: first, it is suppressing the population of box orbits (Barnes & Hernquist 1996), because the gradient of the potential in the centre is very steep and orbits which come close to the centre, that is, box-like, are scattered on centrophobic, that is, tube-like orbits (Gerhard & Binney 1985). Secondly, the gas particles themselves settle into a disc-like configuration. Both processes work towards a v–h_3 correlation more in agreement with what is found in real galaxies (NJB06).

As the light carried by particles on short axis tubes is important for the correct correlation, and as the gas particles move mostly in the *XY* plane we want to test how a different stellar M/L would affect our results. We endorse a very simple method by giving more weight to the gas particles relative to the stellar particles. To assign

realistic M/L we use the results of Bruzual & Charlot (2003) for a stellar population of solar metallicity $Z = 0.02$, Salpeter initial mass function and in the *K* band. A 2-Gyr-old population of such stars would have a M/L$_K$, which is 2.527 lower and 5-Gyr-old population a M/L$_K$ which is 1.336 times lower than a 10-Gyr-old population. The '10-Gyr population' being the case when stars and gas particles have the M/L$_K$, that is, a normal 'GS' observation. When we multiply the masses with the correction factors we see in Fig. 4 (two bottom rows) that the effect on the maps is minimal, but visible. The peak velocity in the 2-Gyr observation is higher and the iso-velocity contours somewhat more closed, but our conclusions are unchanged.

4.4 Kinematic twists and misalignment

A galaxy is kinematically misaligned if its rotation axis is not aligned with its photometric major axis. Because of the strong kinematic misalignment the assumption of a constant position angle is of course wrong. To solve this problem we follow the alternative proce-dure, proposed by K06, and extract the rotation curve by averaging
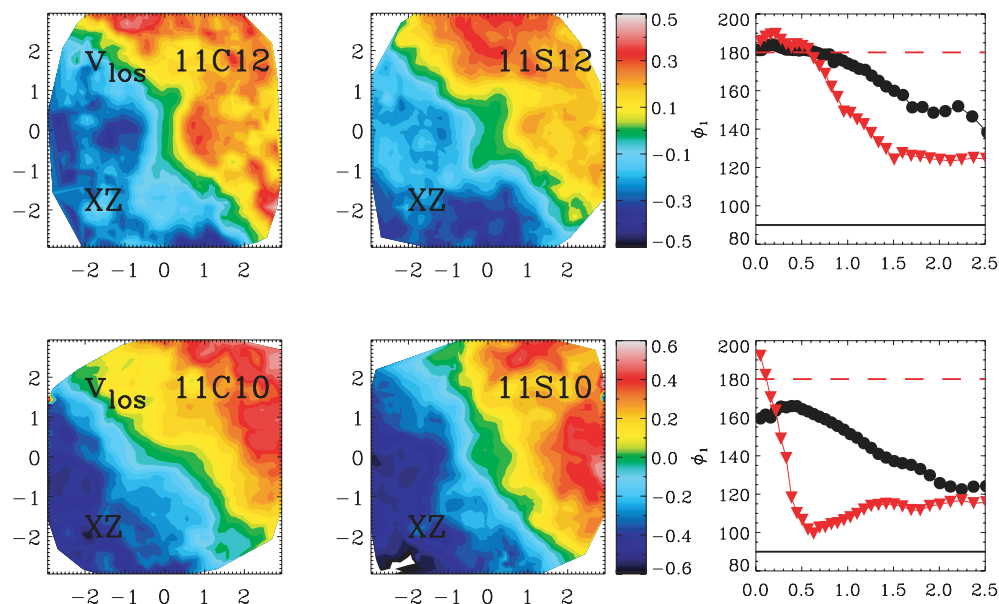
Figure 5. Velocity maps of two 1:1 merger remnants with geometry 10 and 12 of the stars of the collisionless and gaseous remnants (column one and two). Kinematic position angle is shown in the third column for collisionless (black circles) and gaseous (red triangles) remnant. Misaligned rotation (180°) is indicated by a horizontal dashed red line and aligned rotation by a continuous black line. The maps of the collisionless remnants show strong kinematic misalignment (left-hand column), which diminishes at larger radii. The inclusion of gas affects both remnants differently. While the centre of 11S10 exhibits a strong kinematic twist and then almost aligned rotation is the kinematic position angle of 11S12 hardly changed (last column).

over circles (see appendix A of K06). Despite this simplification the authors point out that k_1 and k_5/k_1 are still useful indicators for the bulk motion and deviations from regular motion. But because a circle has no defined position angle, we have to recover the phase angle

$$\phi_1 = \arctan\left(\frac{A_1}{B_1}\right), \tag{4}$$

where the phase angle ϕ_1 represents the direction of the bulk rotation (their equation 10).

By convention signifies a $\phi_1 = 180°$ misaligned rotation and $\phi_1 = 90°$ alignment with the major photometric axis. As shown in the top row of Fig. 5 the collisionless remnant 11C12 is at the centre almost maximally misaligned with a $\phi_1 = 180°$ and slowly changes to about $\phi_1 = 150°$ at larger radii, that is, the remnant has a kinematic twist (KT). This reflects the fact that the fraction of minor axis tubes increases with increasing radius, which skews the rotation more towards the major photometric axis. Nearly the same happens for the gaseous remnant (top row middle panel), only that the strongly misaligned region is smaller, as minor axis tubes are already populated at smaller radii. The KT is slightly more pronounced, to about $\phi_1 = 125°$, between an outer disc-like component and a population of major axis tubes in the centre.

In the second row of Fig. 5 we show an example of another collisionless remnant, 11C10, with slightly lower misaligned rotation ranging from $\phi_1 = 160°$ to $125°$. Interestingly, if resimulated with gas (11S10), the stellar remnant shows a changed kinematic structure with respect to the collisionless remnant. The misalignment is almost completely removed. It is evident that the gas has to overcome a stronger centrifugal barrier in the remnant 11S12 which partially prevents it to sink to the centre and reorganize the orbital structure of the remnant. In remnant 11S10 this is not true and the gas manages to accumulate in the *XY* plane rearranging the shape of the remnant. This is an indication that very strong misalignment

can survive some degree of dissipation while small kinematical misalignment is wiped out more easily.

4.5 The flattening of iso-velocity contours

K06 argued with the example of four early-type galaxies taken from the SAURON sample that different kinematic flattenings, q, show to what extent a galaxy is an axisymmetric rotator, in which case q remains constant with radius (see their fig. 7). Two of their galaxies show peculiar flattenings, one with a radially rising q and one with very wide opening angles in the centre (NGC 2549), but dropping to $q = 0.4$ at larger radii.

As the q profile of NGC 2549 reminds us of flattenings found in 3:1 remnants, we will study in this section the influence of gas on the q-parameter in our 3:1 merger remnants. Their kinematics are much simpler than in 1:1 remnants, because it is much more difficult to populate major axis tube orbits in a 3:1 merger remnant and hence their KTs are almost negligible. Also, all of them show significant rotation in most of the projections, which is a precondition to apply the kinemetric analysis. We analyse the *YZ* and the *XZ* projection, that is, edge on projections, of every remnant. To get an overview of how the q-parameter changes with projection and with the inclusion of gas, we calculate the mean q for every radial bin and compare four subsamples: 3:1 collisionless *YZ* and *XZ* projections and 3:1 dissipational mergers *YZ* and *XZ* projections. We can see in Fig. 6 that the iso-velocity contours of the *XZ* projection of the collisionless remnants have in general a smaller opening angle in the outer regions than for the *YZ* projection, reflecting the more extended, boxy shape of the minor axis tubes for the *YZ* projection (NJB06). The stellar remnants, whose progenitors had a gaseous component, are almost axisymmetric and therefore the flattenings are not very different between the two projections. It is, however, evident from the plot that the q of the stars in the gaseous remnants is significantly lowered at radii smaller than two effective radii. Interestingly for large radii
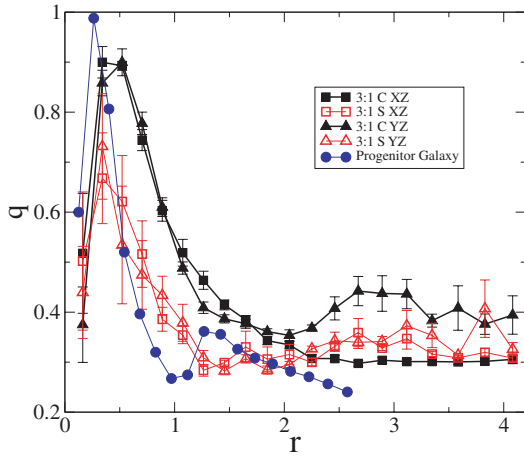
Figure 6. Flattening, q, of the iso-velocity contours versus radius. The q parameter has been averaged at each radial bin for all 3:1 remnants for four cases: 3:1 collisionless merger *XZ* and *YZ* projections and 3:1 gaseous merger *XZ* and *YZ* projections. Error bars indicate the rms at each bin. For comparison we plot the kinematic fit of a progenitor disc galaxy.

we find slightly larger opening angles in the gaseous remnants as compared to the *XZ* projection of the collisionless remnant. This is probably because at large radii the surviving part of the progenitor disc dominates the rotation and the flattening of the initial disc is very low as indicated in Fig. 6 (blue line).

4.6 Systems with polar rings

A particularly interesting 1:1 remnant is shown in Fig. 7. In this case the gas forms a large scale gas ring which is inclined by $\Gamma = 95°$ with respect to the photometric major axis of the galaxy and a

central gaseous disc. The kinematic analysis reveals the different amount of rotation in the gas and in the stars. As the gas ring is very narrow we extract the rotation curve along an ellipse with a $q = 0.3$ and with the same alignment, that is, $\Gamma = 95°$, as the ring. As apparent from the bottom left-hand panel of Fig. 7 already in the collisionless remnant does a significant fraction of stars move on polar orbits. The gas also seems to have a higher line-of-sight bulk motion than the stellar component.

The polar ring is the result of the initial conditions of this particular merger for which initially the discs of the progenitors are inclined to each other by nearly 90°. The properties of this remnant are similar to those of polar ring galaxies. Bekki (1998) has shown that such systems can form in galaxy merging events. Our simulations differ insofar that both progenitor discs have gas and that we ran a larger sample of disc inclinations. Only in two out of 16 1:1 mergers was a significant amount of gas deposited in a polar ring. Typically this is just 10 per cent of the initial gas mass or 1 per cent of the total baryonic mass of the system. The gas in such a polar ring stems from one of the merging partners only. We do not find any significant polar ring structures in 3:1 mergers.

Observed polar ring galaxies, though, have a comparable amount of mass in the polar ring and in the central component, typically an S0 galaxy (see e.g. Sparke & Cox 2000). Our simulations already start with too little gas (10 per cent of the total mass) to form such a system. Alternatively, such systems can form by cold accretion (Macciò et al. 2006) in a cosmological context.

4.7 Counter-rotating cores

The detection of KDCs at the centre of early-type galaxies is an important indication for the hierarchical assembly of elliptical galaxies. A subset of these is the central stellar subsystem, which rotates in the opposite direction to the outer stellar body, so-called CRCs. However, the exact process of how material, supposedly a leftover from a
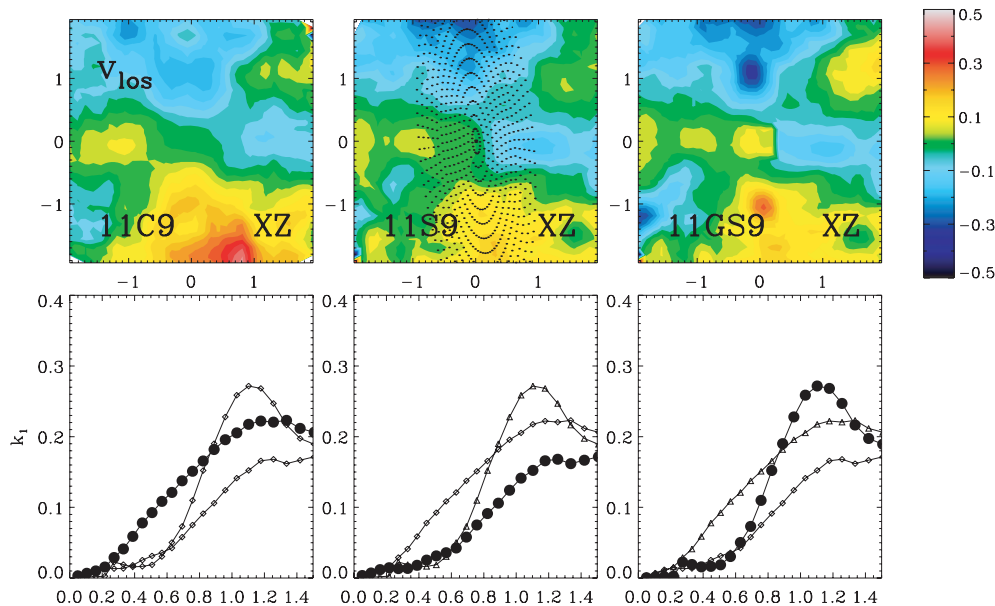

Figure 7. Top row: Edge on projection (along the intermediate axis) of the 2D Velocity fields of 11C9, 11S9 and 11GS9. The rotation curve was extracted along ellipses with $q = 0.3$ and $\Gamma = 95°$ and are overplotted in the top middle panel. Gas settles in a ring with a diameter of about two effective radii, inclined by 95° with respect to the main stellar body. The signature is similar to polar ring galaxies. Very little mass is contained in the polar gas ring itself. Bottom row: The polar rotational structure is already present in the collisionless remnant (bottom left-hand panel, the bulk rotation of the corresponding map above is marked by thicker symbols). The gas ring shows a higher rotation than the stellar component in the gaseous remnant.

merger, retains memory of its original angular momentum vector is a matter of debate. Kormendy (1984) proposed that a dwarf satellite under certain pre-conditions can survive the tidal field of the more massive progenitor and sink to the centre. Balcells & Quinn (1990) then showed in *N*-body simulations that such a formation scenario for a CRC is viable for certain encounter geometries. It was demonstrated by Hernquist & Barnes (1991) that dissipation can play an important role in forming central counter-rotating components (but see also Balcells & González 1998). Barnes (2002) elaborated on these findings, but pointed out that for the same encounter geometry ($i_1 = 71°$, $\omega_1 = 90°$, $i_2 = -109°$, $\omega_2 = 90°$), but for a wider orbit no CRC is formed. The exact reason remains elusive. However, kinematically misaligned gaseous components were commonplace in their simulations, especially for retrograde encounters.

Similarly we find kinematically misaligned gas, counter-rotating or otherwise, in about 50 per cent of the 1:1 merger remnants, but in only 1 out of 32 3:1 remnants. Our best example for a CRC in the *gas* is the merger remnant 11GS16, which originates from a very similar merging geometry ($i_1 = 60°$, $\omega_1 = 90°$, $i_2 = -109°$, $\omega_2 = 71°$) than the original Hernquist & Barnes (1991) calculation. In Fig. 8 we show edge on 2D velocity maps of this remnant. Kinemetry is uniquely suited to analyse maps with KDCs. K06 showed a very instructive example of a set of two-component test models in which they vary the alignment of the central component from aligned ($\Delta\Gamma = 0°$) to counter-rotating ($\Delta\Gamma = 180°$) (their fig. 2) and proved that the size and alignment of the KDC can be easily measured by kinemetry. We take advantage of this and extract the kinemetry of the stellar component of the gaseous remnant, of the gas and stars with identical M/L and of gas and stars with the gas particles having a lower M/L ('2-Gyr-old population').

Observing the gas–CRC at later or earlier times is crucial for the detectability in the maps. While kinemetry does pick up the signal
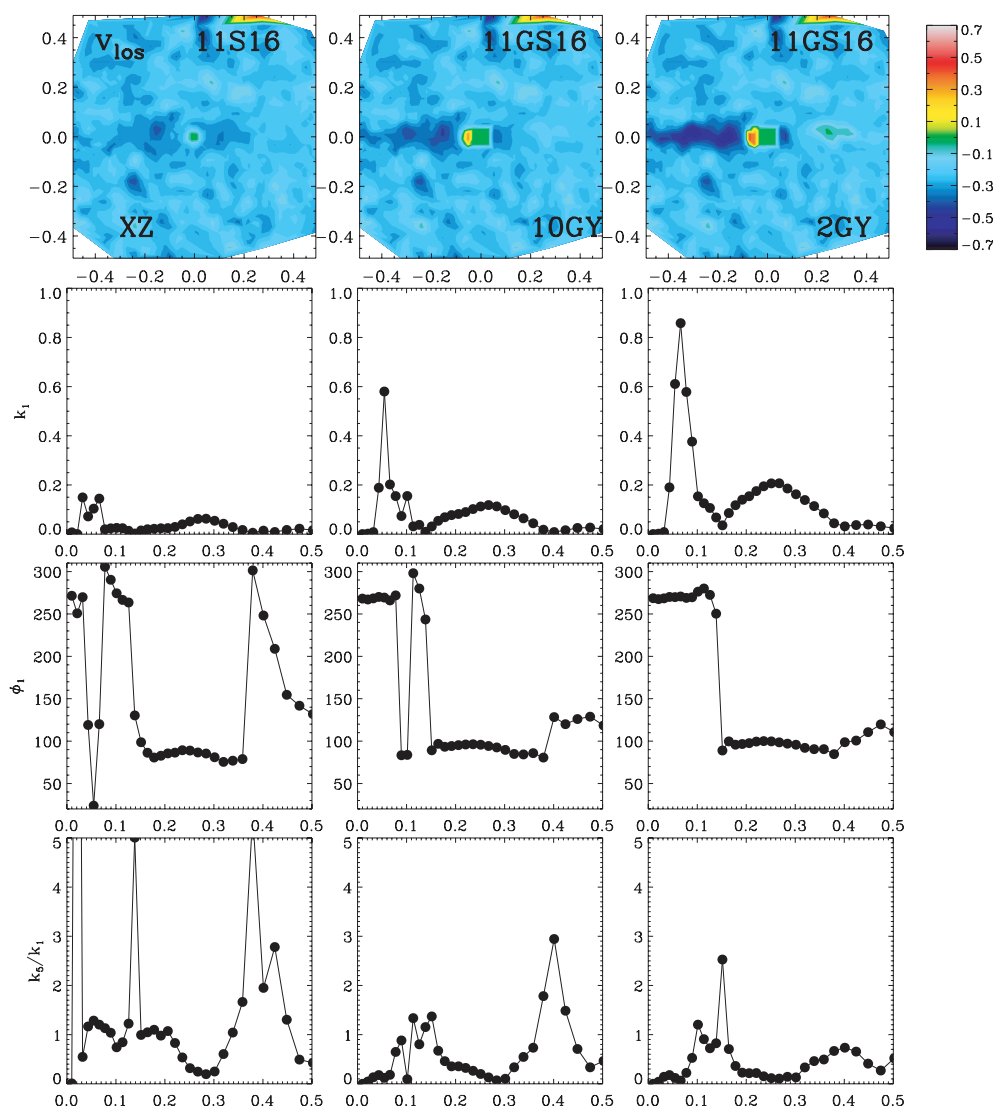

Figure 8. Top row: 2D velocity maps of the 11GS16 with a counter-rotating gas disc in the centre. The old stellar component (left-hand panel), as well as the gas and stars with the same M/L (middle panel) and lower M/L for the gas particles (right-hand panel) are shown. The kinemetry is extracted along ellipses with $q = 0.3$ and $\Gamma = 0°$. Second row: The peak of the rotation curve (k_1) and the visibility of the CRC is improving from left- to right-hand panel. The CRC is hardly visible in the old stellar component. Third row: The 180° kinematic position angle change is best visible in the 2-Gyr-old population map. A second hump is visible at $r \approx 0.4$ and is a sign for the lopsidedness of the outer gas disc. Bottom row: Again the 2-Gyr map shows the clearest transition signature in k_5/k_1.

in the '10-Gyr' observation (Fig. 8, middle column), the '2-Gyr' map shows that the possibility for an observer to find this CRC would be much better. Interestingly the old stellar component is marginally dragged along into counter-rotation, although a weak signal is detectable. This CRC is relatively small, about 10 per cent of the effective radius and the outer disc is lopsided. The CRC is formed in this particular remnant due to a preservation of the original spin alignment of the progenitor discs. The rotation of particles which belonged to either disc 1 or disc 2 in the corresponding, that is, originating from the same merging geometry, *collisionless* remnant are counter-rotating. Apparently in the dissipational remnant does the gas component of one progenitor galaxy lose more angular momentum than the other and settle in a fast spinning disc in the centre.

However, the most clearly visible and largest CRCs are found in the old *stellar* component of equal-mass merger remnants. 11S6 is such an example and its maps and kinematry are shown in Fig. 9. We can neither detect a CRC in the collisionless remnant (top left-hand panel), nor in the gas (top right-hand panel), but only in the 'old stars' (top middle panel). The CRC has a size of approximately half an effective radius and shows all telltale signs in the kinematry, for example, $180°$ change of kinematic position angle. It is also visible in the h_3 showing an anticorrelation with v_{los} as would be expected from a axisymmetric system with regular rotation. To study this phenomenon closer we examined the four distinct stellar components from which the particles which build up the CRC can consist: disc of galaxy 1, bulge of galaxy 1, disc of galaxy 2 and bulge of galaxy 2. In Fig. 10 (top) we illustrate that the most strongly counter-rotating components are the particles from the disc and the bulge belonging originally to the *same* galaxy (the particles of galaxy 2 lost most of their rotation and lie between those two extremes). We found it instructive to examine the evolution of the angle between the spin vectors of the bulge particles of galaxy 1 and the other three stellar components, respectively the two other gas components. We calculate the angular momentum vector of each component with respect to its own centre of mass. In the same Fig. 11, left-hand panel, we see that the alignment of the spin of the counter-rotating bulge changes suddenly around $t = 90$, which is shortly after the second, and final, encounter (around $t = 70$). The bulge seems to be impulsively removed from its own disc. Later evolution shows that counter-rotation is slightly increasing and the angle difference stabilizes at $-150°$ to $-180°$. Only a significant part of the second bulge is at later times dragged into counter-rotation as well. This process is not occurring in all the remnants. The spin vector of all components, gas or stellar, of the remnant 11GS3 (Fig. 11, right-hand panel) are aligned and no CRC is visible in the maps.

The formation of a CRC in such a context opens up questions if this is a robust result if realistic modes of star formation are included or if the subsequent merging history preserves such a KDC. Some aspects of forming a CRC in the old stellar component are favourable in light of recent observations and are discussed in Section 5. These issues are beyond the scope of this paper and we try to address them in a subsequent paper.

4.8 Line-of-sight velocity dispersion

The 2D velocity dispersion maps of elliptical galaxies of the SAURON sample show a richness of features, which are even less understood than velocity maps in terms of their formation history. Some of the galaxies show low dispersion regions, mostly in the centre. Drops in σ are indicative that dissipation has played a role in the formation of the galaxy. It is indeed a very good indicator

because lower velocity dispersion means that locally entropy has been taken out of the system and that would be hard to imagine in a pure collisionles process. However, collisionless mergers can still produce non-trivial velocity dispersion maps as is shown in Fig. 12. The merger remnant 11C1 has a high σ disc-like feature, which is a result of the peculiar merging geometry ($i_1 = 0°$, $\omega_1 = 180°$, $i_2 = 0°$, $\omega_2 = 0°$), that is, both progenitors are in the same plane and have anti-aligned angular momentum. The two superposed counter-rotating 'discs' in the final remnant maximize the line-of-sight velocity dispersion. In contrast the merger 11C3 shows a more typical flat dispersion profile. Both remnants have a dispersion dip in the centre, but this signature is a leftover from the cold centres of the initial Hernquist bulges (Hernquist 1990). Also the velocity maps are quite different for both remnants. While the two counter-rotating components in 11C1 compensate each other, resulting in almost zero v_{los}, does the remnant 11C3 show normal rotation. The high-σ disc phenomenon is probably rare, as 11C1 is the only remnant in our sample who has this feature, which is no surprise as the merging set-up needs to be rather fine-tuned.

Merger remnants with gas show a much wider variety in their velocity dispersion maps. We illustrate this with the example of a 1:1 and a 3:1 merger remnant (Fig. 13). The dissipation in the 3:1 remnant (bottom row) leads to a cold disc-like component, which imprints a dumbbell like velocity dispersion structure. In general gaseous discs in unequal-mass mergers settle into the equatorial plane, extend to larger radii and have more rotation than in equal-mass mergers. The kinematry shows that line-of-sight dispersion is lower than in the collisionless remnant at almost all radii (same figure, bottom right-hand panel). Quite the contrary happens in the merger 11GS4, where a fraction of the gas particles accumulate into a high dispersion ring at about an effective radius from the centre. Because the biggest fraction of the gas, like in all simulations, settles into a compact, dynamically cold, central disc, the dispersion map shows a double-peak structure (Fig. 13, top row). The peaks being edge-on cuts through the torus-like structure of the gas at this radius. The dissipation at this radius actually causes an increase the velocity dispersion with respect to the collisionless remnant (same figure, top right-hand panel).

Also face-on (*XY*) views of gaseous remnants have distinctive features, such as ring-like depressions in the velocity dispersion (top row of Fig. 14). The most interesting aspect is that this feature is also imprinted by the gas in the old stellar component. The low dispersion is not more pronounced If gas and star particles are observed simultaneously (11GS2), however the central gas component appears even colder in the map. The depression in σ corresponds to a positive h_4 indicating a LOSVD that is more peaked than a Gaussian (same figure, bottom row).

5 COMPARISON TO OBSERVATIONS

The previous sections highlighted the diversity of 2D maps of various moments of the LOSVD. We want to discuss in this section, how these results relate to observations of real early-type galaxies, for example, to the results of EM04. Unfortunately this comparison is mainly qualitative, although we will loosely refer to the kinematric categories as suggested by K06. For each category we will refer to the galaxies which are the principal examples for this category and comment on their possible merger origin.

Low rotation. The kinematry of the remnant 11C5 (Fig. 3), shows (scaled) rotation of below 10 km s^{-1} inside one effective radius, which is extremely low rotation. There are many galaxies in the SAURON sample that are not rotating outside a fast rotating central
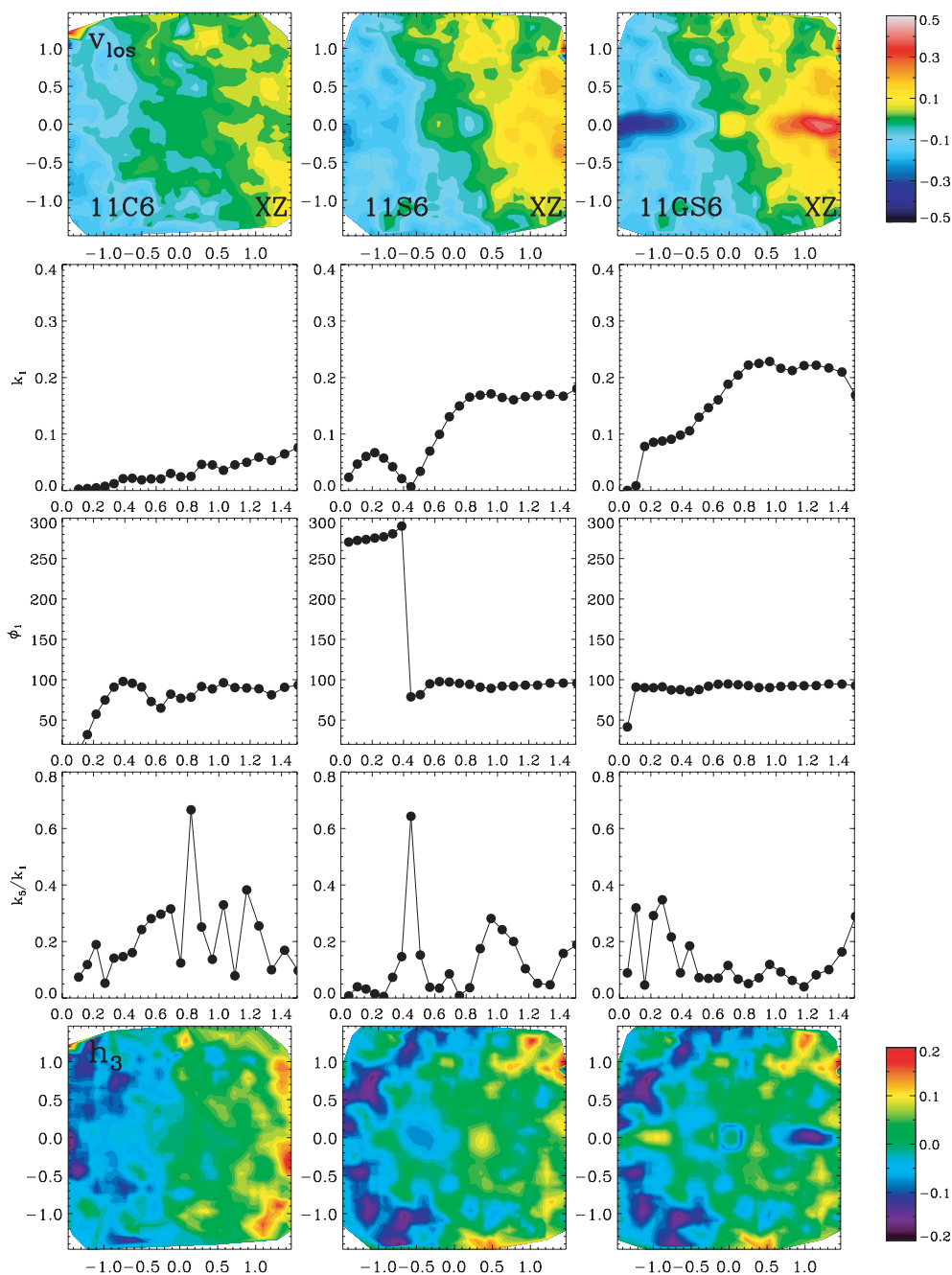
Figure 9. Top row: projected 2D line-of-sight velocity in the *XZ* projection for the collisionless remnant (11C6), the stellar remnant of the counterpart with gas (11S6) and including the gas (11GS6) component assuming that all gas turned into stars after the merger was complete (from left- to right-hand panel). In the middle panel a counter-rotating stellar core (CRC) is clearly visible. In the right-hand panel the kinematic signature of the thin disc appears. The ellipses, which have a $q = 0.5$ and $\Gamma = 0°$, along which we extracted the rotation curves are overplotted. Second row: Rotation curves, k_1, extracted along an ellipse with $q = 0.5$ and $\Gamma = 0°$ centred on the photometric major axis. The curves are shown for the collisionless remnant (11C6), gas and stars of the dissipative remnant (11GS6) and the stellar component of the gaseous remnant (11S6), which has a CRC. Third row: For 11S6, the ratio k_5/k_1 shows a strong peak at the transition radius between the CRC and the outer spheroid, as found in the test examples of K06. The other curves show no distinct features. Fourth row: Reconstructed angular direction ϕ_1 of the rotation, k_1. 11S6 shows a CRC with almost exactly 180° misalignment in its rotation (i.e. counter-rotation). Bottom row: 2D distribution of h_3 for the same remnants. Strong signatures for the CRC and the thin disc (middle and right-hand panels).

KDC, the so-called slow rotators (Cappellari et al. 2005). We find three examples of galaxies with a rotation below 20 km s^{-1}: NGC 4374, 4486 and 5846. All these objects are round and have elliptical or slightly boxy isophotes. Their high central velocity dispersion indicates that they are fairly massive and that a merger of two very massive late-type galaxies would be needed to destroy the rotation in the progenitors and increase the mass accordingly. The scenario of merging elliptical galaxies would be even more favourable, as already the progenitors would have very little rotation (Naab et al. 2006b).

Kinematic twists and misalignment. A KT is indicated by a smooth change of the kinematic position angle. We find KTs only in
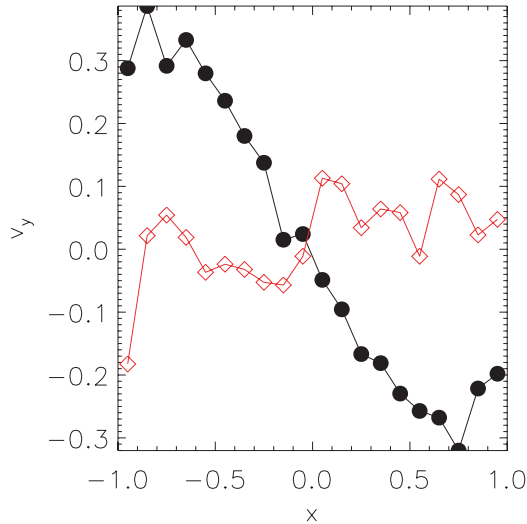
Figure 10. Line-of-sight velocity averaged in a thin slit along the major axis at the end of the simulation of remnant 11S6. The particles originally belonging to the disc of galaxy 1 (black filled circles) show a clear counter-rotation with respect to the particles originally belonging to the bulge of the same galaxy (open diamonds).

1:1 mergers which are violent enough to scatter stars from minor axis tubes on to major axis tube orbits. More than half of the 1:1 merger remnants show, at least at the centre, iso-velocity contours twisting more than $30°$. The frequency and amplitude in the simulated equal-mass merger remnants seems to be higher than for the KTs found in the SAURON sample. In contrast, 3:1 mergers do not produce any galaxy with a twist of more than $20°$, be it with or without gas. In this respect 3:1 mergers are in better agreement with observations.

Counter-rotating cores. We define CRCs as a subgroup of KDCs with a sudden KT of $180°$. We find no CRCs in 3:1 remnants with or without gas and we find counter-rotating populations in two 1:1 collisionless remnant, but which are not compact enough to pass as a core. For the stellar component of the 1:1 simulations with gas, we find at least four candidates for CRCs from the maps: 11S4, 11S6, 11S13 and 11S14 and one in the gas 11GS16. McDermid et al. (2006) found in the SAURON galaxies two distinct types of KDCs: slow rotators harbour large KDCs (kpc scale) with ages

and metallicities similar to the main body of the galaxy and fast rotators have smaller (below kpc scale) and younger KDCs. Our simulations imply that stellar CRCs in slow rotators are formed in 1:1 mergers when gas is present and, consistent with observations, as these CRCs consist of 'old' star particles in the simulation, they would not be detected as a distinct population, for example, the CRC appears old. Additionally the main body would rotate slower, if he has formed from a 1:1 merger. CRCs formed in the simulations in the gas are much smaller and younger, again in agreement with observations, but we can hardly form them in 3:1 mergers. Most KDCs in fast rotators are actually CRCs, which might be a bias in the observations (see discussion in McDermid et al. 2006), still they seem too common place and merger simulations need to answer how to form them and maintain a high rotation in the main body.

The v–h_3 correlation. Collisionless simulations show that there is generally a positive correlation between these quantities in the centre of the remnants (NJB06). The presence of gas would inhibit the population of box orbits, the orbit class responsible for positive correlations (see discussion in Section 4.3). Contrary to what is seen in the collisionless remnants, we see no correlation of v–h_3 in the centre of any galaxy in the SAURON sample. In the outer parts there are a few examples with positive correlations: NGC 1023, 2699, 4270 and particularly NGC 4526. This could be an indication for a presence of bars (Chung & Bureau 2004). This argues (see NJB06) against pure collisionless mergers as possible formation mechanism of rotating SAURON galaxies, in agreement with the discussion on CRCs, see above.

Opening angle of iso-velocity contours. In Section 4.5 we showed that on average 3:1 merger remnants with open iso-velocity contours have had less dissipation. This is because dissipation causes flat discs and an overall more flattened and axisymmetric potential. As more material now rotates in the equatorial plane, the iso-velocity contours are closing resulting in a smaller q. This result can not be easily compared in a statistical way to observations. Therefore we have chosen a pair of galaxies, which in the range of the SAURON observations have the same ellipticity ϵ and the same v/σ: these are NGC 7457 and 4660, with $\epsilon = 0.44$ and $v/\sigma = 0.6$ (Cappellari et al. 2005). Although these galaxies appear in the v/σ–ϵ diagram at the same position, we find that the velocity maps of EM04 of these two galaxies look very different: the velocity contours in NGC 7457 are much more open than those for NGC 4660. This indicates that much more dissipation was present in the formation of NGC 4660,
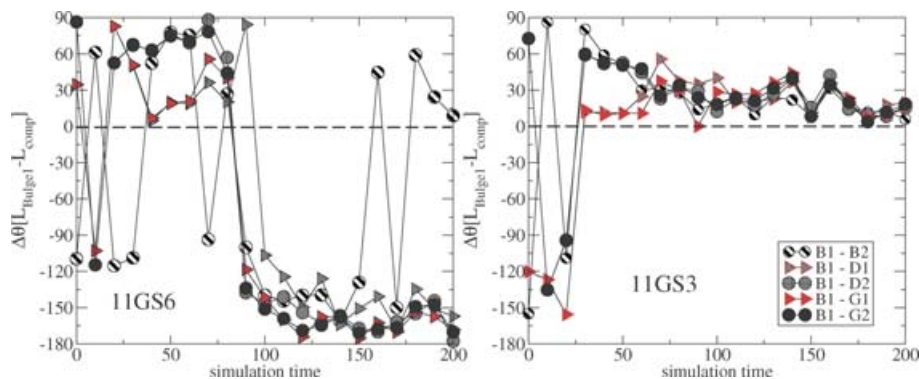

Figure 11. Left-hand panel: evolution of the angle between the angular momentum vector of bulge 1 particles of remnant 11S6 and all other components: D1 (disc 1), B2 (bulge 2), D2 (disc 2), G1 (gas disc 1) and G2 (gas disc 2). Alignment is indicated by the thick horizontal black line at $0°$. The spin of the bulge 1 is suddenly changed shortly after the second and final passage and stays at almost $-180°$ with respect to all other components. Only the particles of bulge 2 seem to evolve secularly and become more counter-rotating with time. Right-hand panel: the same properties plotted for remnant 11GS3, which has no CRC. The spin angles of all dynamical components are aligned shortly after the merging process.
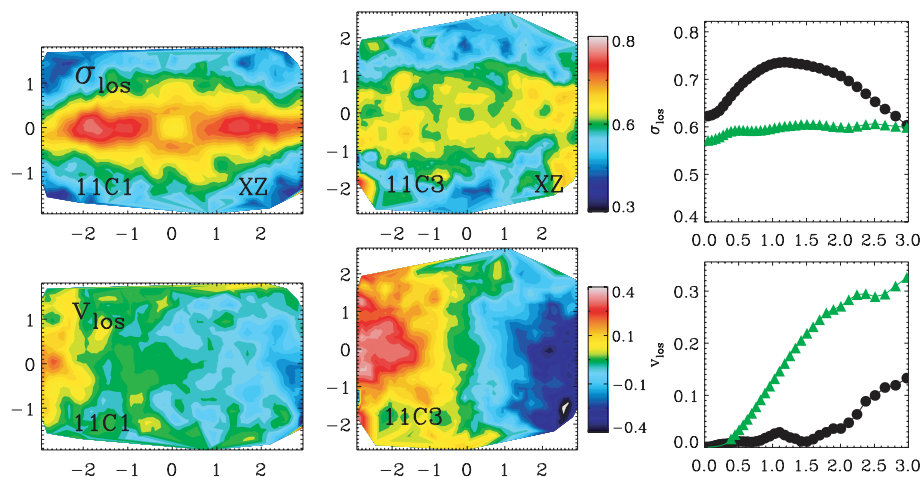
Figure 12. Top row: velocity dispersion of two collisionless 1:1 merger remnants 11C1 and 11C3. The remnant 11C1 has a high velocity dispersion disc-like component, as can be seen from the kinemetric profiles (black circles, right-hand panel), significantly higher than 11C3 (green triangles). Bottom row: because 11C1 originated from an in-plane merger of two discs with opposite spins is almost no net rotation visible. 11C3 shows regular rotation.
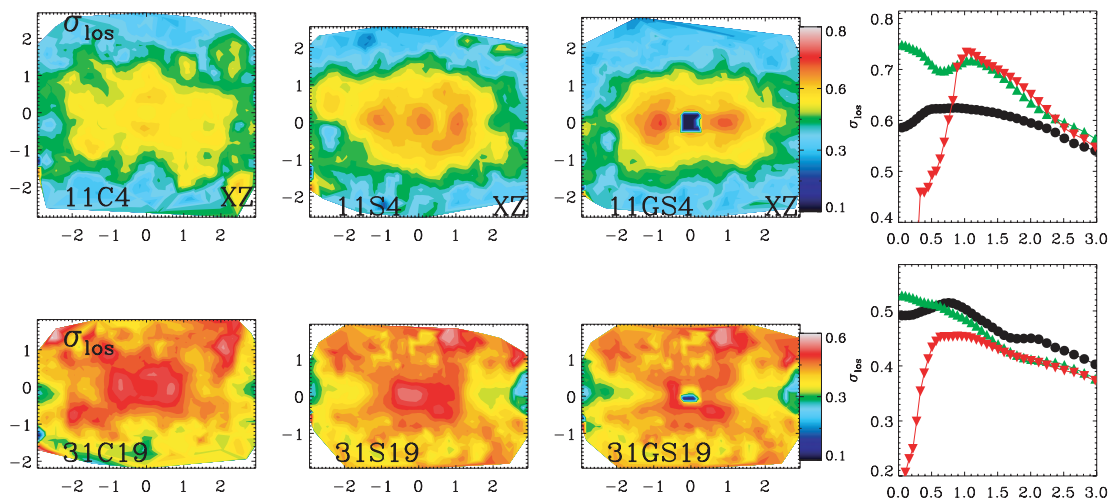

Figure 13. Top row: the velocity dispersion maps of the *XZ* projection for the 1:1 merger with merging geometry 4. The velocity dispersion of the collisionless merger, 11C4, shows a slight depression of σ_{los} at the centre. The dispersion field of the stellar component of the gaseous remnant, 11S6, shows an off-axis double peak, which is even stronger if the gas particles are taken into account (11GS4). The kinemetry velocity dispersion extracted along an ellipse with $q = 0.3$ is shown in the most right-hand column for 11C4 (black circles), 11S4 (green triangles) and 11GS4 (red upside down triangles). Inclusion of the bottom row: in the 31GS19 the gas settles partly into a cold stellar disc, which causes a *V*-shaped depression in the velocity dispersion.

probably causing a flattened disc-like component in this galaxy. The ellipticity in the outer parts, from the RC3 (de Vaucouleurs 1991), also is very different: 0.41 for NGC 7457 and only 0.21 for NGC 4660. This gives support for the presence of a second flattened component in the middle of NGC 4660. For NGC 7457 we can not infer its intrinsic flattening, but it is likely to be constant with radius, since the ellipticity profile is constant (Peletier & Balcells 1997).

Polar rings. As laid out in Section 4.7, we find one very pronounced polar ring in the merger 11GS9. This polar ring is present in simulations with or without gas. In the SAURON survey the only two examples of polar rings are NGC 2685 and 2768. Both polar rings are only visible in the gas (Sarzi et al. 2006). The radial extent of the polar ring in the merger is very similar to what is found in these two observations. There appears to be a fundamental difference between simulations and observations, as no stellar polar ring is found in the data. The statistics, however, is very small, so no strong conclusions

can be drawn here. There are observational cases known of stellar polar rings (e.g. NGC 4365 Surma & Bender 1995; Davies et al. 2001), but these are generally small, not going as far out as one effective radius.

Low-σ rings. In some equal-mass merger remnants with gas we find ring-like depressions in σ, mainly for face-on projections. Without gas we do not find them at all. Such a feature has been reported for one SAURON elliptical galaxy only: NGC 5813. In the spiral galaxy NGC 4314 (Falcón-Barroso et al. 2006) a similar situation is visible: a star formation ring with a low gas velocity dispersion and a high stellar dispersion. In a recent survey of six nearby Seyfert galaxies (Barbosa et al. 2006) with IFU-GMOS, three of the galaxies, NGC 2273, 3227 and 4593, show ring-like depressions in σ in varying strength. If such low σ rings are signatures of previous merging, it is interesting to note that most of them are found in active galaxies.
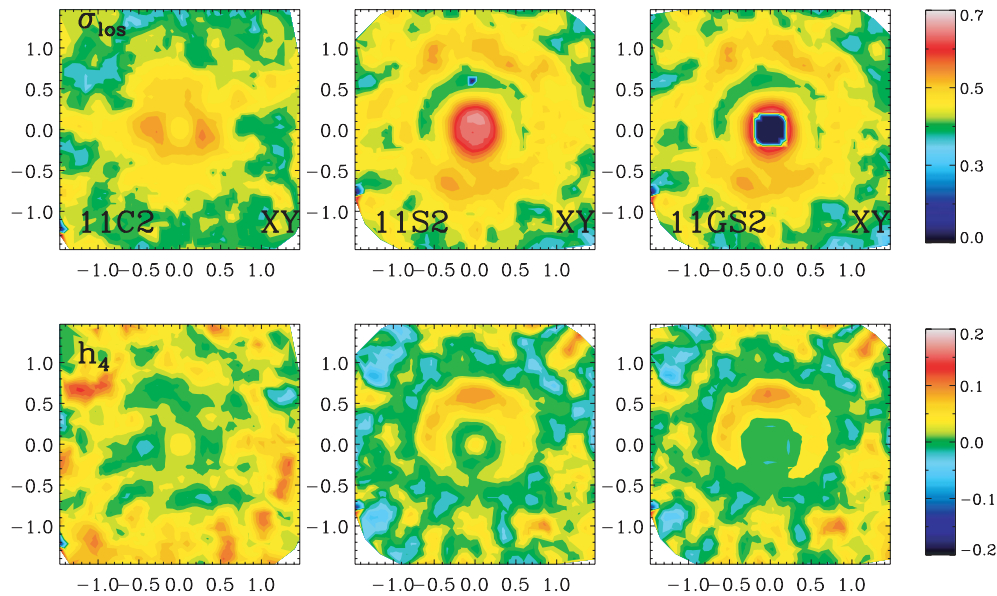
Figure 14. Projected 2D velocity dispersion for remnant 11S2 (top row) the 2D distribution of h_4 for the same projections (bottom row). A depression of σ at about $0.5r_e$ is clearly visible. In the same region h_4 changes sign and becomes positive indicating a LOSVD more peaked than a Gaussian.

Central σ drops. In almost all merger remnants which were formed from progenitors with a dissipational component, a significant fraction of the gas falls to the centre, showing a very low σ_{los} in the maps. In contrast, the velocity dispersion of the stars is increasing towards the centre. In general the SAURON observations for early-type galaxies also show peaks in σ in the centre, in agreement with the simulations. There are a few objects with a central minimum in the velocity dispersion: these are NGC 4382 and 2768. For spiral galaxies, recently Ganda et al. (2006) and Falcón-Barroso et al. (2006) found that dips in the central velocity dispersion are common, and that their frequency goes up with increasing Hubble type. They conclude that these dips are caused by central discs. In the case of the ellipticals the stars need about 1 Gyr to dynamically heat up after formation (Wozniak et al. 2003). So we suspect that in these two galaxies the velocity dispersion dips are caused by young stars. For NGC 4382 this could be consistent with the line-strength maps measured by Kuntschner et al. (2006), but this idea does not work for NGC 2768 for which old populations are inferred in that paper. In this galaxy there must have been a different mechanism to keep the stars in the central region cold. This would be consistent with the centre of some Sa galaxies, where velocity dispersion dips are found which are old (Peletier et al. 2007).

Other σ features. We found one example for a high σ disc-like (11C1) structure caused by counter-rotation in the merger remnants. This feature is also rare in galaxies, NGC 4473 being the only example in the SAURON survey (NGC 4550 might also be comparable, but has a more overall complex structure). A merger origin seems very plausible for such a system although 11C1 has no net rotation and NGC 4473 has still some. But the set-up of the merging discs gave them identical amount of rotation with opposite sign which is very unlikely to happen in nature, such that some net rotation might well survive a similar merging geometry. NGC 2549 and especially NGC 3384 have dumbbell structures in their velocity dispersion maps and NGC 3377 has a strong low σ disc. All these galaxies are fast-rotating, which fits well with our results,

that we find such discs predominantly in 3:1 mergers. However, we find them more abundantly than seen in EM04. The merger origin of NGC 2685 has been proposed before (Hau, Carter & Balcells 1999). We add circumstantial evidence to this picture on the basis of the formation of a double-peaked velocity dispersion structure in some equal-mass mergers. The dissipational component and the violence of the merging seem to be of the essence to puff-up stars and gas simultaneously.

In general, collisionless remnants show bigger opening angles of the iso-velocity contours, more boxy isophotes, velocity dispersion profiles without central peaks, no strong anticorrelation between v and h_3. Remnants with a dissipational component show smaller opening angles of the iso-velocity contours for the same ellipticities (inclinations), strong dips in the gaseous velocity dispersion profile and an anticorrelation between v and h_3. Additionally CRCs are more common in equal-mass mergers than in mergers of unequal mass. We conclude that globally the non-rotating subset of the representative SAURON sample of local galaxies agrees better with our 1:1 merger simulations, while the rotating subset can be reproduced by the dissipational 3:1 merger remnants.

6 SUMMARY AND CONCLUSIONS

We presented 2D maps of various moments of the LOSVDs of a large sample of 1:1 and 3:1 disc merger remnants with and without gas. Every remnant was resimulated with a dissipational component containing 10 per cent of the luminous mass, allowing us to assess the influence of gas on the 2D fields. Additionally we performed a kinematric analysis using the method devised by K06 to quantify properties such as kinematic position angle or deviations from regular rotation.

The difference between equal-mass and an unequal-mass merger remnants is not only seen in photometric and global kinematic properties (Naab, Burkert & Hernquist 1999), but also in the 2D kinematics (Bendo & Barnes 2000), which exhibits very different

features. 1:1 mergers can lead to a merger remnant with low rotation. Also, orbit classes rotating around the major axis of the remnant can only be populated in significant numbers in 1:1 mergers, leading to kinematic misalignment and twists, while 3:1 remnants rotate much faster and have almost no KTs. All rotating collisionless mergers fail to reproduce the observed $v - h_3$ anticorrelation, because the population of box orbits in the centre is not inhibited (NJB06).

The presence of a dissipative component of only 10 per cent of the luminous disc mass in the progenitors can lead to a considerable change in the properties of 1:1 remnants. They are more round, kinematic misalignment is reduced, CRCs are forming and KTs are more pronounced. Rare but observed features like polar gas rings form also in equal-mass mergers. The effect of gas on 3:1 remnants is less dramatic. KTs, CRCs and polar rings are not formed or at least must be very rare. A noticeable change is that the opening angles of the iso-velocity contours become smaller. As shown in NJB06, the $v - h_3$ anticorrelation is now much better reproduced, especially if the gas component is included in the analysis.

Merger remnants show a variety of velocity dispersion features. Significant central velocity dispersion dips are caused by infalling gas. The central star component in the gaseous runs, however, is heated. Edge on gas discs can exhibit lower velocity dispersion (as found in 3:1 remnants) or edge-on gas rings can produce double-peaked velocity dispersion maps (as found in 1:1 remnants). Gaseous structures can imprint a ring-like depression in σ even on the stellar component, which is also visible in h_4.

2D analysis of LOSVDs of *N*-body simulations of galaxy formation are an additional tool to connect the formation history of galaxies with their observable kinematic fine structure. We defer a full statistical analysis to future work, with a larger sample of galaxies mergers, which will also take star formation into account.

The simulations and analysis presented her are a step forward in understanding the possible formation of ellipticals by mergers of discs. We focus on the influence of a small dissipative component, which is important to understand its impact on the dynamical properties of the remnants. However, additional physical processes like star formation and feedback will change the detailed properties especially at the centre of the remnants (Mihos & Hernquist 1996; Springel, Di Matteo & Hernquist 2005) and definitely have to be considered for simulations with higher gas fractions (Robertson et al. 2004; Springel & Hernquist 2005). We believe that the global effects of dissipation even with star formation will be very similar to the results presented here. However, larger gas fractions might result in more massive stellar discs in the remnant. From a kinematic point of view disc merger remnants appear very similar to observed ellipticals, although questions regarding the age and metalicity of the stellar populations have to be addressed in the future. Analytical models of disc formation (Naab & Ostriker 2006) as well as semi-analytical modelling (Khochfar & Silk 2006a) in combination with merger simulations (Naab et al. 2006b) can be used to place further constraints on the disc merger hypothesis.

ACKNOWLEDGMENTS

REFERENCES

Bacon R. et al., 2001, MNRAS, 326, 23
Balcells M., González A. C., 1998, ApJ, 505, L109
Balcells M., Quinn P. J., 1990, ApJ, 361, 381
Barbosa F. K. B., Storchi-Bergmann T., Cid Fernandes R., Winge C., Schmitt H., 2006, MNRAS, 371, 170
Barnes J. E., 1992, ApJ, 393, 484
Barnes J. E., 1998, in Saas-Fee Advanced Course 26: Galaxies: Interactions and Induced Star Formation Dynamics of Galaxy Interactions. Springer-Verlag, Berlin, p. 275
Barnes J. E., 2002, MNRAS, 333, 481
Barnes J. E., Hernquist L., 1996, ApJ, 471, 115
Bekki K., 1998, ApJ, 499, 635
Bender R., Saglia R. P., Gerhard O. E., 1994, MNRAS, 269, 785
Bendo G. J., Barnes J. E., 2000, MNRAS, 316, 315
Bournaud F., Combes F., 2003, A&A, 401, 817
Bruzual G., Charlot S., 2003, MNRAS, 344, 1000
Cappellari M. et al., 2005, in Nearly Normal Galaxies in a LCDM Universe. A Conference Celebrating the 60th Birthdays of George Blumenthal, Sandra Faber and Joel Primack. UC Santa Cruz, Santa Cruz
Chung A., Bureau M., 2004, AJ, 127, 3192
Cretton N., Naab T., Rix H.-W., Burkert A., 2001, ApJ, 554, 291
Davies R. L. et al., 2001, ApJ, 548, L33
de Vaucouleurs G., de Vaucouleurs A., Corwin H. G., Jr, Buta R. J., Paturel G., Fouqué P., 1991, Third Reference Catalogue of Bright Galaxies. Springer Verlag, New Yark
Emsellem E. et al., 2004, MNRAS, 352, 721 (EM04)
Falcón-Barroso J. et al., 2006, MNRAS, 369, 529
Ganda K., Falcón-Barroso J., Peletier R. F., Cappellari M., Emsellem E., McDermid R. M., Tim de Zeeuw P., Carollo C. M., 2006, MNRAS, 367, 46
Gerhard O. E., 1993, MNRAS, 265, 213
Gerhard O. E., Binney J., 1985, MNRAS, 216, 467
Hau G. K. T., Carter D., Balcells M., 1999, MNRAS, 306, 437
Hernquist L., 1990, ApJ, 356, 359
Hernquist L., 1992, ApJ, 400, 460
Hernquist L., 1993, ApJS, 86, 389
Hernquist L., Barnes J. E., 1991, Nat, 354, 210
Jesseit R., Naab T., Burkert A., 2005, MNRAS, 360, 1185 (JNB05)
Khochfar S., Burkert A., 2003, ApJ, 597, L117
Khochfar S., Burkert A., 2006, A&A, 445, 403
Khochfar S., Silk J., 2006a, MNRAS, 370, 902
Khochfar S., Silk J., 2006b, ApJ, 648, L21
Kormendy J., 1984, ApJ, 287, 577
Krajnović D., Cappellari M., de Zeeuw P. T., Copin Y., 2006, MNRAS, 366, 787 (K06)
Kuntschner H. et al., 2006, MNRAS, 369, 497
Macciò A. V., Moore B., Stadel J., 2006, ApJ, 636, L25
McDermid R. M. et al., 2006, MNRAS, 373, 906
Mihos J. C., Hernquist L., 1996, ApJ, 464, 641
Naab T., Burkert A., 2001a, in Funes J. G., S. J., Corsini E. M., eds, ASP Conf. Ser. Vol. 230, Galaxy Discs and Disc Galaxies. Astron. Soc. Pac., San Francisco, p. 451
Naab T., Burkert A., 2001b, ApJ, 555, L91
Naab T., Burkert A., 2003, ApJ, 597, 893 (NB03)
Naab T., Ostriker J. P., 2006, MNRAS, 366, 899
Naab T., Trujillo I., 2006, MNRAS, 369, 625
Naab T., Burkert A., Hernquist L., 1999, ApJ, 523, L133
Naab T., Jesseit R., Burkert A., 2006a, MNRAS, 372, 839 (NJB06)
Naab T., Khochfar S., Burkert A., 2006b, ApJ, 636, L81
Peletier R. F. et al., 2007, in Vazdekis A., Peletier R.F., eds, Proc. IAU Symp. 241, Stellar Populations as Building Blocks of Galaxies. Cambridge University Press, Cambridge, in press (astro-ph/0702256)
Peletier R. F., Balcells M., 1997, New Astron., 1, 349
Robertson B., Yoshida N., Springel V., Hernquist L., 2004, ApJ, 606, 32
Sarzi M. et al., 2006, MNRAS, 366, 1151

Sparke L. S., Cox A. L., 2000, in Combes F., Mamon G. A., Charmandaris V., eds. ASP Conf. Ser. Vol. 195, Dynamics of Galaxies: From the Early Universe to the Present. Astron. Soc. Pac., San Francisco, p. 119

Springel V., Hernquist L., 2005, ApJ, 622, L9

Springel V., Di Matteo T., Hernquist L., 2005, ApJ, 620, L79

Surma P., Bender R., 1995, A&A, 298, 405

Toomre A., Toomre J., 1972, ApJ, 178, 623

van der Marel R. P., Franx M., 1993, ApJ, 407, 525

Wozniak H., Combes F., Emsellem E., Friedli D., 2003, A&A, 409, 469

APPENDIX A: 2D VELOCITY MAPS AND KINEMETRIC DATA OF MERGER REMNANTS

This is a selection of 2D velocity maps of all the remnants. We have to restrict ourselves to the *XZ* projection, which is best suited for a kinematric analysis, as it shows the highest rotational amplitude. For the equal-mass mergers we analyse the maps by extracting the rotation curve along circles, as the kinematic twists are too strong (Figs A1, A2 and A3). Although we do not study projection effects, we can see the merger-to-merger variance of the kinematric parameters, such as the kinematic misalignment in 1:1 mergers (Fig. A4) and the presence of counter-rotating cores (Fig. A5). A full list of the orbital parameters for all merging geometries is given in Table A1.

The maps of 3:1 merger remnants are much more regular and the appearance of the maps with and without gas does not change dramatically, although the isovelocity contours are more closed if gas is included in the simulations (Figs A6, A7 and A8).

Table A1. Full list of merging geometries. For unequal-mass mergers the first number indicates the orientation of the more massive galaxy as i_1 and ω_1, the second number indicates the orientation of the more massive galaxy as i_2 and ω_2.

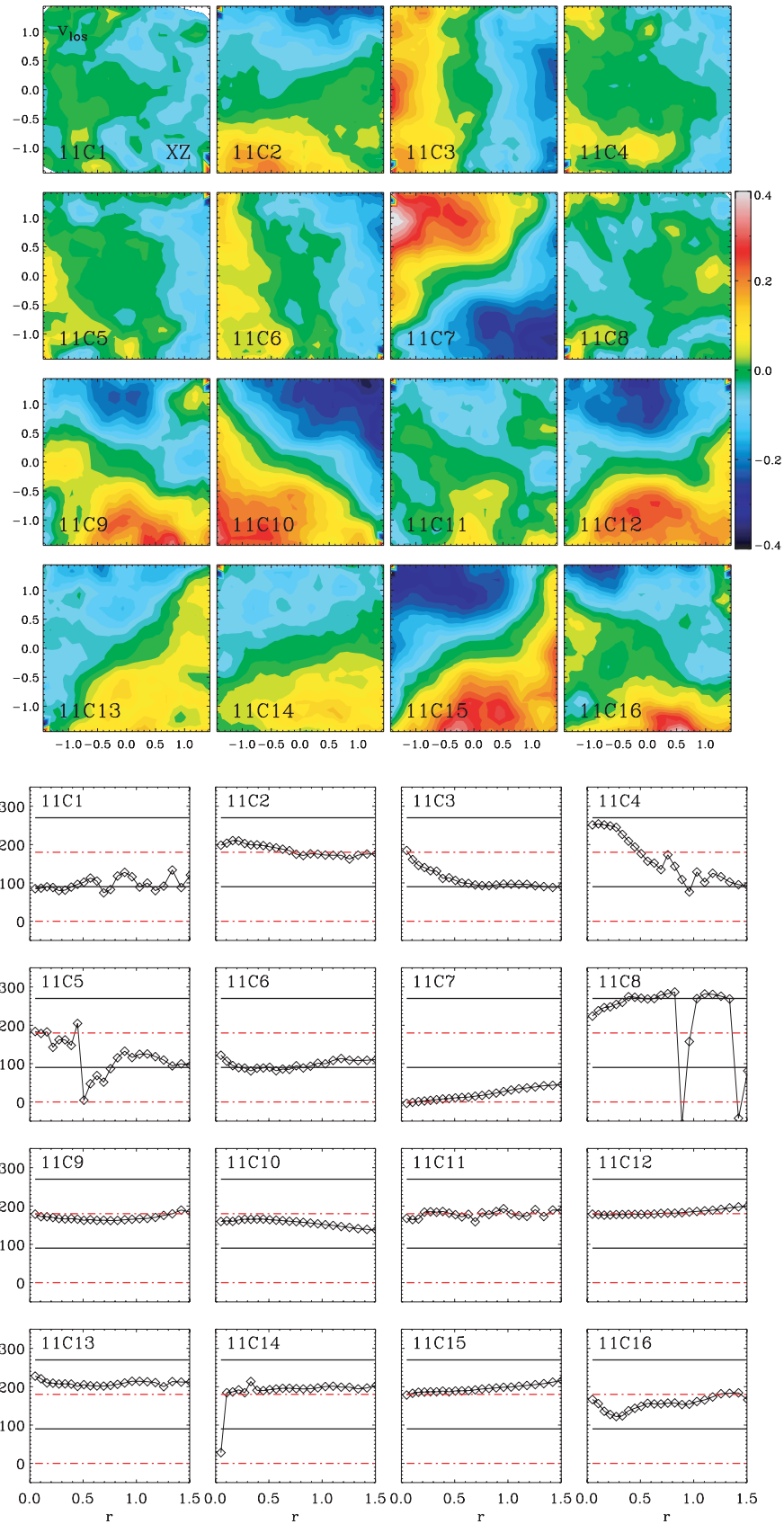| Geometry	i_1	i_2	ω_1	ω_2
1/17	0	0	180	0
2/18	0	0	71	30
3/19	0	0	71	−30
4/20	0	0	71	90
5/21	−109	−60	180	0
6/22	−109	−60	71	30
7/23	−109	−60	71	−30
8/24	−109	−60	71	90
9/25	−109	0	180	0
10/26	−109	0	71	30
11/27	−109	0	71	−30
12/28	−109	0	71	90
13/29	−109	60	180	0
14/30	−109	60	71	30
15/31	−109	60	71	−30
16/32	−109	60	71	90

Figure A1. Top: velocity maps for the collisionless 1:1 remnants for the *XZ* projection. Bottom: corresponding kinematic position angles extracted along circles. By definition kinematic position angles of 90° and 270° signify rotation which is aligned with the photometric major axis (indicated by straight black lines), correspondingly 0° and 180° indicate maximally misaligned rotation (red dot–dashed lines). Strong kinematic misalignment is present in almost all remnants.
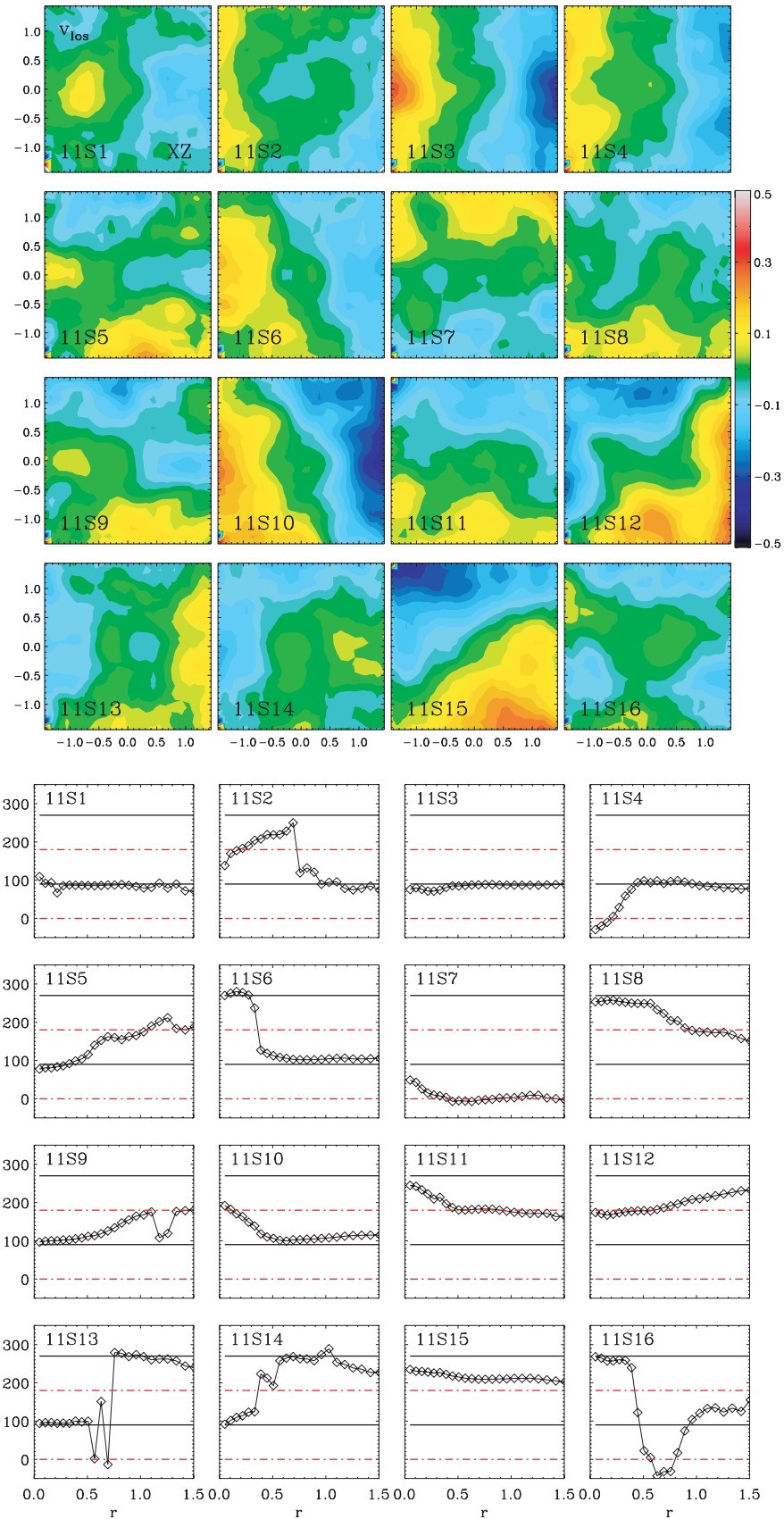
Figure A2. Top: velocity maps for the stellar component of the 1:1 remnants which had progenitors with a gas component. Bottom: corresponding kinematic position angles. Definition for horizontal lines as before. Sudden KTs give indications for kinematic decoupled components in the centre of the remnants. In the outer parts the remnants are more aligned than their collisionless counterparts (see Fig. A1).
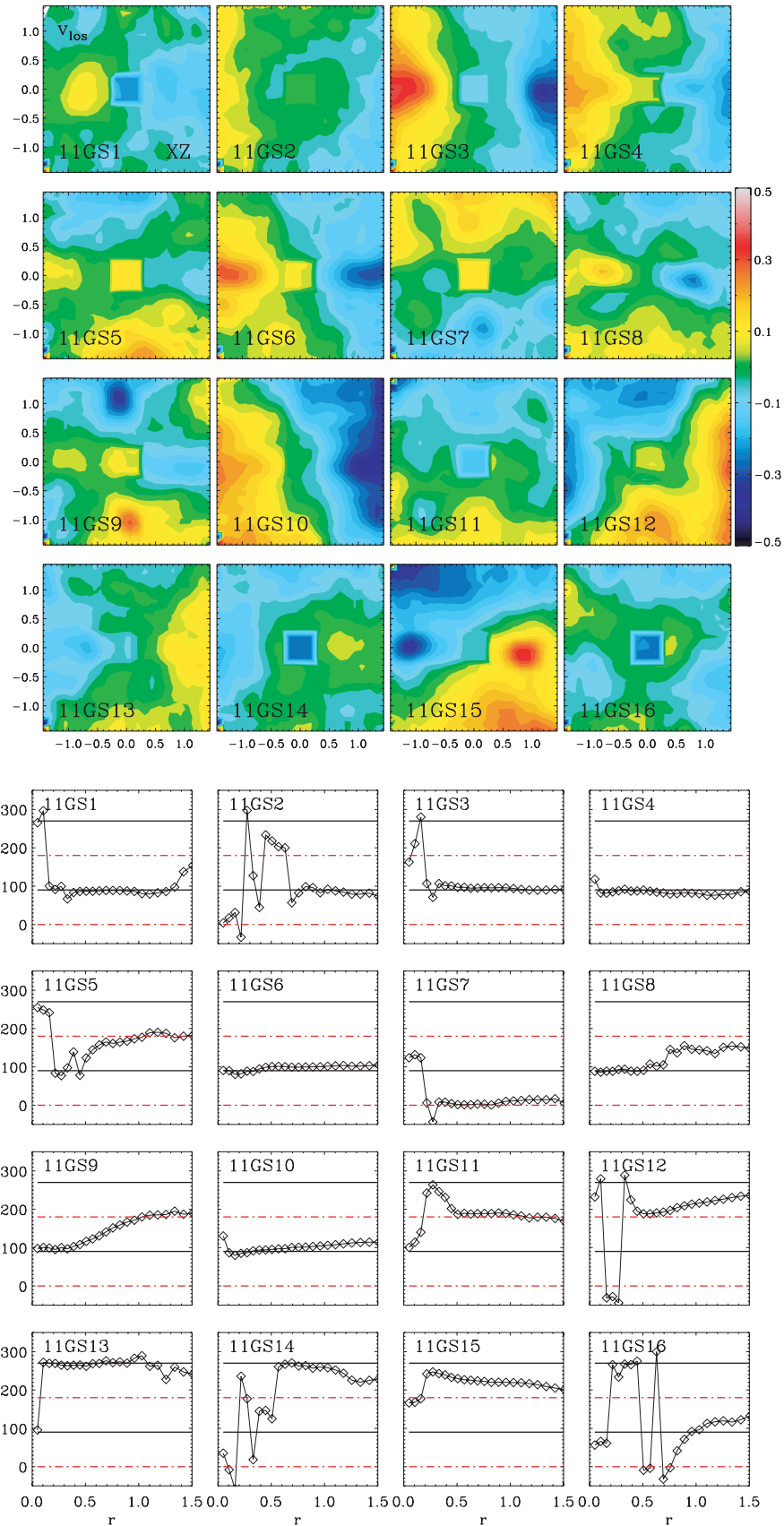
Figure A3. Top: velocity maps of the same 1:1 remnants like in the previous figure, but with the gas particles converted into stars. Bottom: kinematric position angles as before. Overall misalignment is reduced, some KDCs are not visible anymore, as the gas dominates the centre.
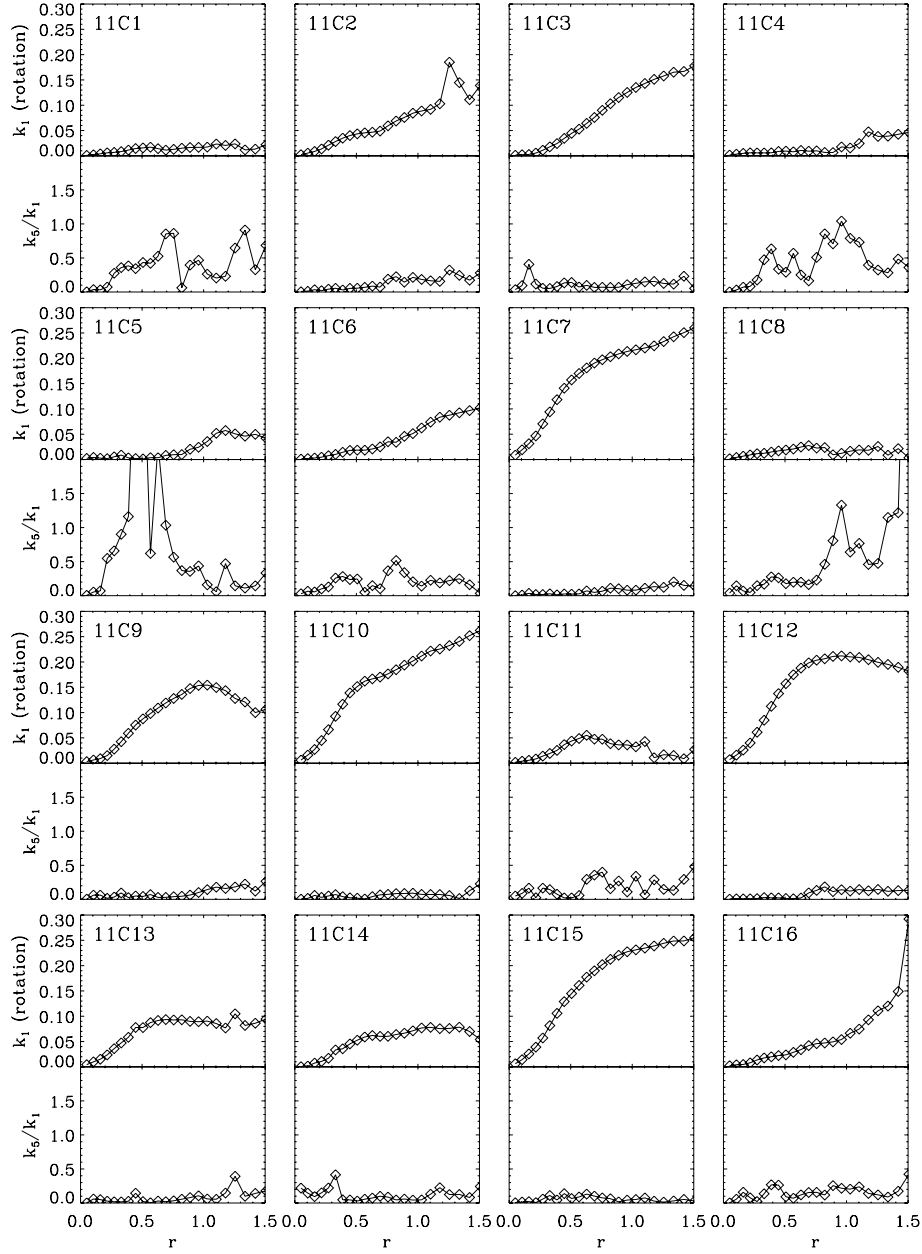
Figure A4. The k_1 term (bulk rotation) and the k_5/k_1 (deviation from regular rotation) are plotted with a common *x*-axis. The low rotation of 11C5, due to a high box orbit fraction in this remnant causes a high k_5/k_1 ratio.
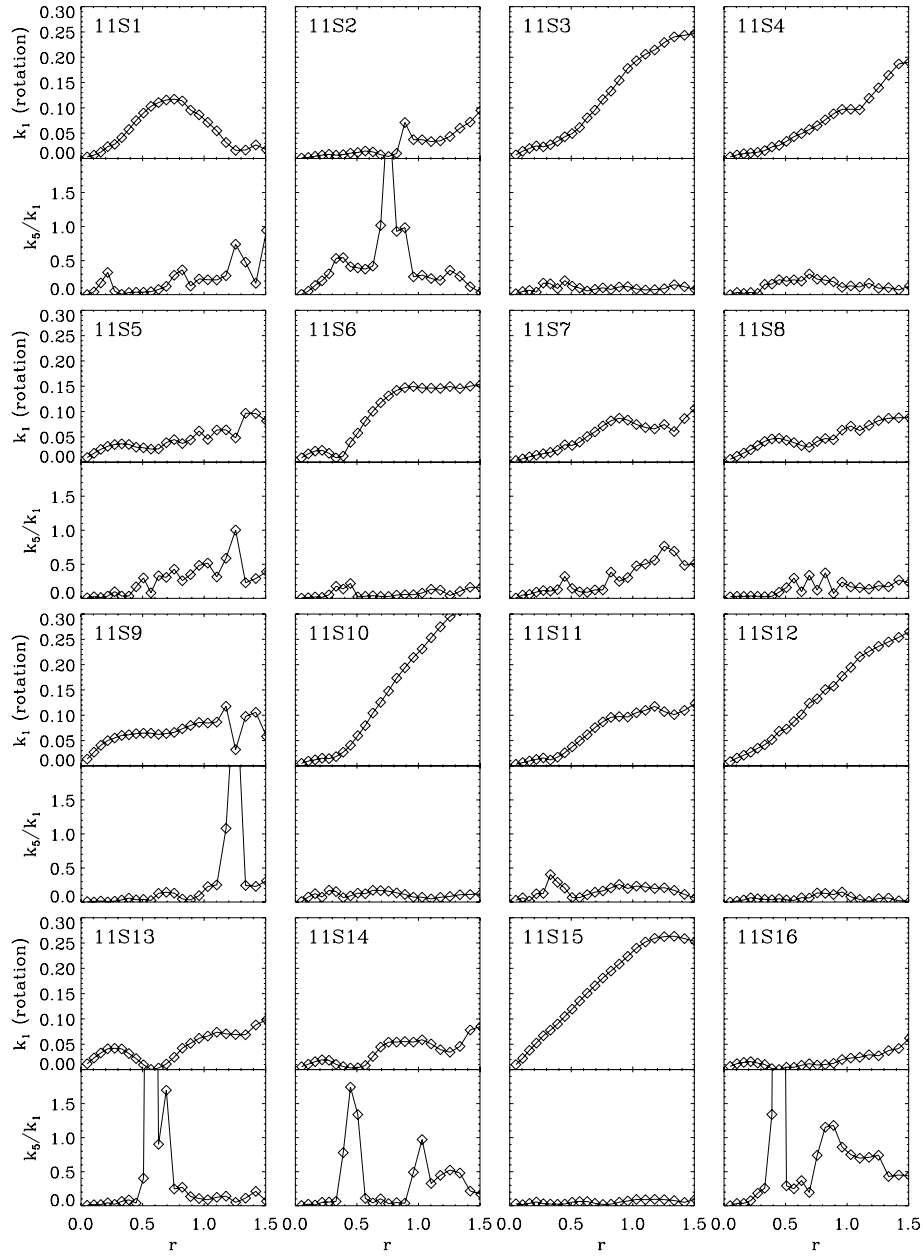
Figure A5. The k_1 (bulk rotation) profiles and the k_5/k_1 ratio for the stellar component of remnants with gaseous progenitors. Some CRCs are clearly visible in 11S6, 11S13, 11S14 and 11S16 in both a sudden peak in k_5/k_1 and in the double hump structure of k_1.
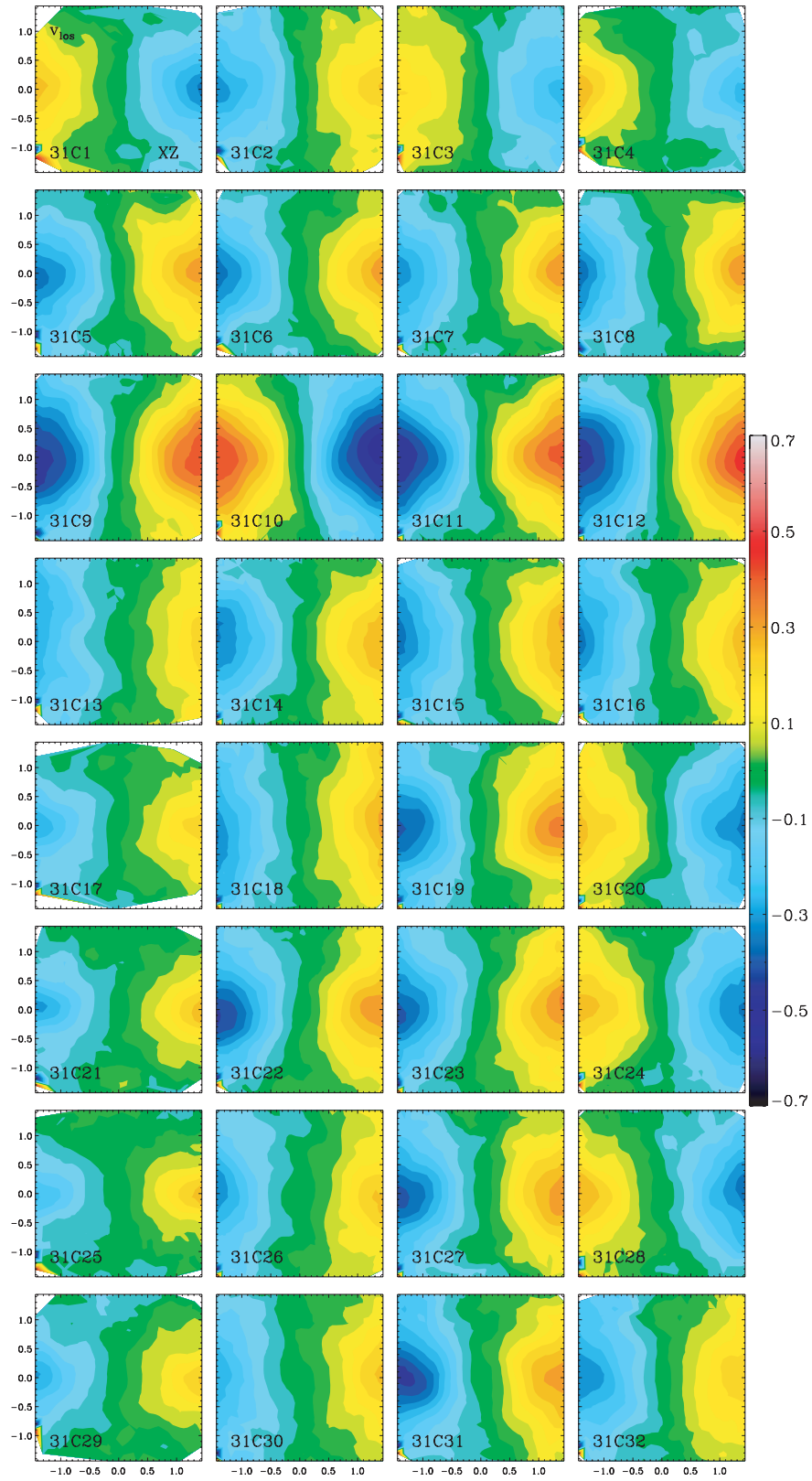
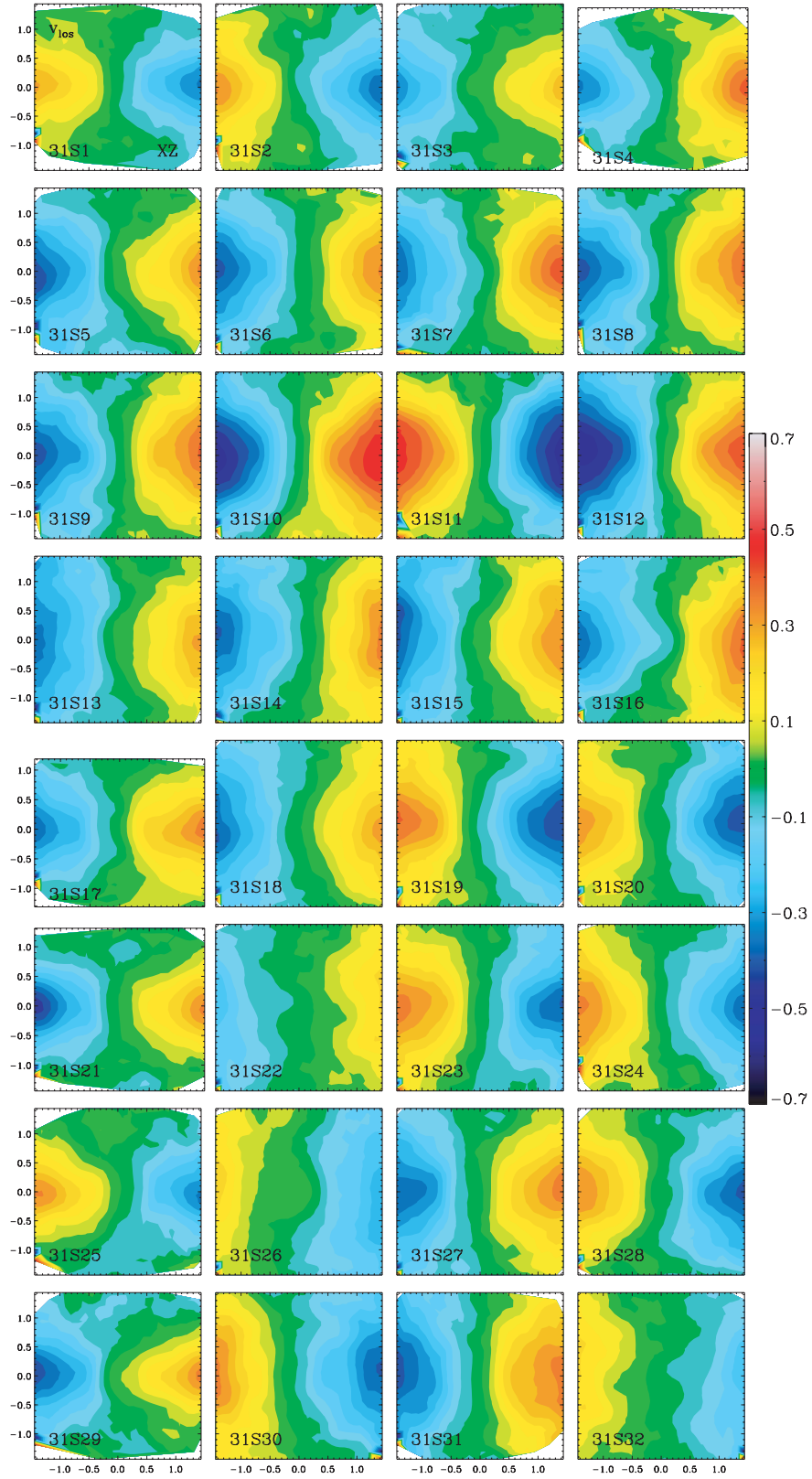**Figure A6.** Velocity maps for the collisionless 3:1 remnants for the *XZ* projection.

Figure A7. Velocity maps for the stellar component of the 3:1 remnants which had progenitors with a gas component.
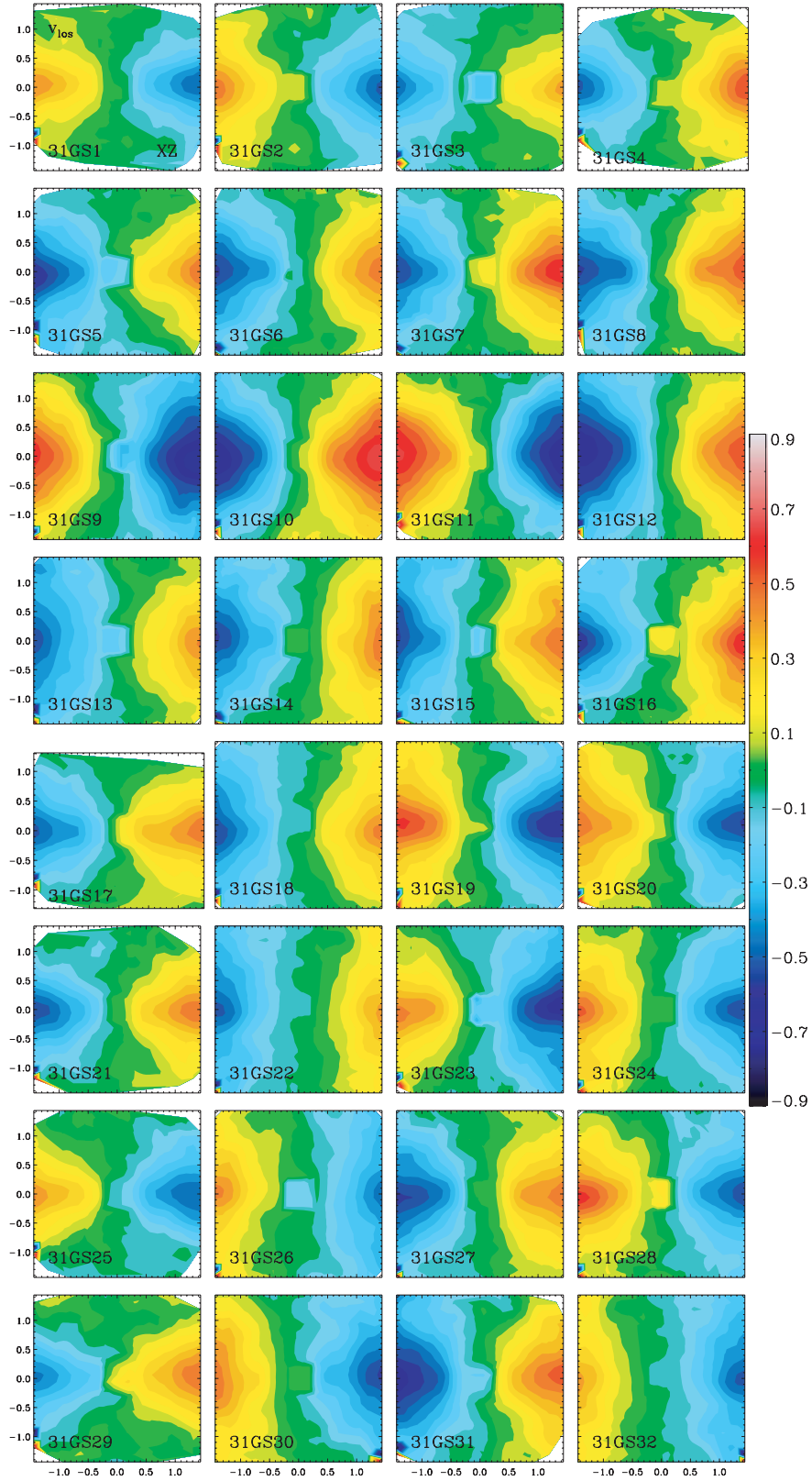
Figure A8. Velocity maps of the same 3:1 remnants like in the previous figure but with the gas particles converted into stars.

This paper has been typeset from a TEX/LATEX file prepared by the author.